Faculty of Physics and Astronomy
University of Heidelberg

Diploma thesis
in Physics

submitted by
Klaus Klingmüller
born in Bonn, Germany

Heidelberg
2004

Pair Production on the Worldline

This diploma thesis has been carried out by
Klaus Klingmüller
at the Institut für Theoretische Physik

under the supervision of
Dr. Holger Gies
and
Prof. Michael G. Schmidt

Paarproduktion auf der Weltlinie
Zusammenfassung

Die Paarproduktion ist als nichtlineares, nichtperturbatives Phänomen der Quantenfeldtheorie sowohl von theoretischem als auch von experimentellem Interesse. Während im Aufbau befindliche Experimente die Realisierung von e^+e^- Paarbildung in starken elektrischen Feldern in Aussicht stellen, ist die Anwendung der vorhandenen theoretischen Modelle auf Spezialfälle beschränkt. In dieser Arbeit verwenden wir den neuartigen Zugang der Weltliniennumerik, der durch die Kombination von Methoden der String-Theorie mit Monte Carlo-Techniken entstanden ist. Dieser Ansatz führt zu einem numerischen Algorithmus zur Berechnung von Paarproduktionsraten in skalarer QED für beliebige Hintergrundfelder. Wir testen den Algorithmus anhand des klassischen Sauter-Potentials, für das wir zum ersten Mal die lokale Produktionsrate berechnen. Des Weiteren untersuchen wir die Produktionsrate für die Superposition eines konstanten E-Feldes mit einem räumlich oszillierenden Feld in Abhängigkeit von der Oszillationsfrequenz. Unsere Resultate zeigen, dass die Näherung der lokalen Ableitungsentwicklung bereits für kleine Frequenzen scheitert, dass aber stark fluktuierende Felder durch Ableitungsentwicklung für das gemittelte Feld behandelt werden können. Dadurch erhalten wir mit dem Weltlinienbild ein umfassendes Verständnis für die nichtlokale Natur der Paarproduktion.

Pair Production on the Worldline
Abstract

As a nonlinear and nonperturbative phenomenon of quantum field theory, pair production is both of theoretical and experimental interest. While the experimental realization of e^+e^- pair production in strong electric fields is in prospect, the application of existing theoretical approaches is limited to special cases. In this thesis we make use of the recently developed worldline numerics, which combines string-inspired methods with Monte-Carlo techniques. This approach yields a numerical algorithm to compute pair-production rates in scalar QED for arbitrary background fields. We test the algorithm with the classic Sauter potential, for which we compute the local production rate for the first time. Furthermore we study the production rate for a superposition of a constant E field and a spatially oscillating field in dependence on the oscillation frequency. Our results reveal, that the approximation by a local derivative expansion fails already for small frequencies, whereas for strongly fluctuating fields a derivative expansion of the averaged field yields proper results. Thereby we obtain a deep understanding of the nonlocal nature of pair production in the worldline picture.

Contents

Chapter 1

Introduction

Pair production is one of the most striking non-linear phenomena in quantum field theory. It was first proposed for electron-positron pairs in strong temporally and spatially constant electric fields [1, 2, 3]. Today it is often referred to as the Schwinger [4] mechanism. As a nonperturbative mechanism, pair production is of great theoretical interest. From a phenomenological point of view, it corresponds to probing the theory in the domain of strong fields. Consequently we encounter pair production in many topics of contemporary physics, for instance black hole evaporation [5] and e^+e^- creation in the vicinity of charged black holes [6, 7] as well as particle production in hadronic collisions [8] and in the early universe [9, 10]. Since QED pair production in strong fields represents the conceptually simplest case, it can serve as a theoretical laboratory for all these cases.

However, a sizeable rate for spontaneous pair production requires extraordinary strong electric fields. For instance macroscopic or mesoscopic field strengths should be comparable in size to the so-called critical field strength which corresponds to the electron-mass scale, $E_{\mathrm{cr}} = m^2/e \approx 1.3 \cdot 10^{18} \frac{V}{m}$. For a long time it seemed inconceivable to produce macroscopic electric fields of the required strength in the laboratory. With the development of intense optical lasers, in the early 1970's the question was raised whether they have the potential to experimentally study pair production [11]. But until now all disposable optical lasers did not reach the required intensity. Meanwhile the possibility of making use of the strong Coulomb fields evolving in heavy ion collisions has been discussed [12], but no clear experimental signature has been detected yet. Today there are several promising experiments in progress. X-ray free electron lasers (FEL) are under construction, the *Linac*

Coherent Light Source (LCLS) at SLAC [13] and the *TESLA XFEL* at DESY [14, 15]. These X-ray lasers with their high energy and transverse coherence may be focusable down to the diffraction limit in order to obtain electric fields of very high peak intensity [16]. Also the use of optical lasers of the peta-watt class is under discussion [17].

At present, with the prospect of experimental realizations, the topic is of special interest also from the theoretical point of view. Many different methods, such as the proper-time method [4, 18], the canonical method [18], the Schrödinger-Functional approach [19], functional techniques [20, 21], mean-field treatment [22, 23, 24] and instanton techniques [25, 26], have been developed, to study pair production in external fields. Of particular conceptual interest is the computation of the production rate in terms of the effective action for a given background, which is also used in this thesis. Owing to an intimate relation between the effective action and the vacuum-persistence amplitude, it is the imaginary part of the effective action that encodes information about pair production, which, in this context, is interpreted as spontaneous vacuum decay. This approach yields the instantaneous production rate, neglecting back-reactions and memory effects. However, mean-field QED reveals, that the imaginary part of the effective action appears as the source term in quantum-kinetic equations [22, 23, 24]. Consequently, for phenomenology, results based on the effective-action approach can directly serve as input for transport equations, which can take back-reactions and memory effects into account.

Even though the existing methods follow a well defined and technically stringent concept, their application often involves serious technical and conceptual difficulties. Up to now, no reliable and universal method is known, neither analytic nor numeric, to obtain pair-production rates in inhomogeneous electric fields. In standard approaches functional traces have to be evaluated with the knowledge of the spectrum of the corresponding differential operator, which is only available for special cases. Moreover, controlling the divergencies one possibly encounters when summing up the eigenvalues is a delicate task.

In this thesis, we develop a new approach to compute the pair-production rate for inhomogeneous electric fields in scalar quantum electro dynamics (QED). We make use of a recently developed algorithm [27, 28, 29, 30, 31] which is based on the string-inspired *worldline formalism* [32, 33, 34, 35, 36, 37, 38]. The idea of this approach consists of rewriting the functional de-

terminants that we encounter when computing the effective action in terms of one-dimensional path integrals. These paths represent the worldlines of the quantum fluctuations in coordinate space, thereby offering an intuitive picture of the quantum world. The path integrals can then be evaluated numerically with Monte-Carlo techniques. The important advantage compared to other approaches lies in the fact that the worldline algorithm can be formulated independently of any symmetry of the background. The identification of and the summation over the spectrum of quantum fluctuations are done in one single and finite step.

Our efforts will result in a profoundly universal algorithm that we apply to spatially inhomogeneous electric fields. As a result we gain a detailed understanding of the dependence of pair production on spatial field-strength fluctuations. Our findings demonstrate that the pair-production rate for inhomogeneous fields interpolate between two limiting cases: For slowly varying fields, the field strength can be regarded as locally constant, i.e., a derivative expansion in lowest order yields proper results (averaged derivative expansion). By contrast, if the field contains small-scale fluctuations, the pair production is well approximated by averaging out the fluctuations to perform a derivative expansion on the averaged field. Our findings determine quantitatively the transition from the averaged derivative expansion to the derivative expansion of the average, revealing that the latter limit is approached surprisingly rapidly. As a by-product we obtain new results for the local production rate of the classic Sauter potential (the global rate has been evaluated analytically by Nikishov [39] which we rediscover in passing).

The organization of this thesis is as follows. In chapter 2 we present the basic concepts of worldline numerics: The Schwinger functional and the effective action are introduced, in Minkowski as well as in Euclidean space. We proceed with the one-loop computation of the effective action and introduce its worldline representation. It is explicitely derived for both, scalar and spinor QED. At this point we preliminary specialize to scalar QED and describe the numerical realization of the worldline approach, the capability of which is then demonstrated for the example of a constant magnetic field. To compare the numerical values to the analytic result, we also review the derivation of the Heisenberg-Euler effective action. The chapter is concluded with a brief outlook on worldline numerics in spinor QED. Chapter 3 is devoted to the worldline numerical approach to pair production in scalar QED. After pointing out the connection between the effective action and the

pair-production rate, we describe various steps of the development process of our algorithms: At first we address the example of a constant electric field. The Schwinger pair-production is derived and several algorithms of increasing sophistication are developed to deal with different field strengths. The example provides us not only with a better understanding of the details of the worldline numerical approach, but also with a deeper insight into the quantum nature of pair production. All this serves as a preparation for turning to inhomogeneous fields. Considering the Sauter potential as an analytically mastered example configuration, we proceed with the development of our algorithms. The most efficient and flexible algorithm is based on a numerical analysis of a probability distribution function (PDF) for a suitably defined ensemble observable that facilitates the extraction of coherent n-pair-production poles. Using this algorithm, the local pair-production rate is computed and integrated to obtain the total pair-production rate which agrees with Nikishov's result with satisfactory accuracy. Of course, the algorithm is not restricted to the Sauter potential, but is immediately applicable to any spatially inhomogeneous field configuration. In order to perform a systematic study of the influence of inhomogeneities on pair production, we finally consider a superposition of a time independent sine potential and a constant field. By varying the sine frequency, the consequences of inhomogeneity can be studied in quantitative detail. As one of our main results, we discover new nonlocal phenomena in the pair-production rates, that find an intuitive explanation in the worldline picture. Thereby we gain a profound understanding of the dependence of pair production on spatial field fluctuations of different scales.

We conclude with a summary of the results and point out some perspectives for future work.

Chapter 2

Effective Action on the Worldline

2.1 The Effective Action

2.1.1 Minkowski Space

In Minkowski space, the Schwinger functional $Z[J]$ is defined by

$$Z[J] := \int \mathcal{D}\phi \; e^{i \int d^4x \; (\mathcal{L}[\phi] + J\phi)}. \tag{2.1}$$

The integral in the exponent extends over all space-time. To be more precise, the x^0 integration goes from $\lim_{T\to-\infty} T(1-i\epsilon)$ to $\lim_{T\to\infty} T(1-i\epsilon)$ with an infinitesimal small $\epsilon > 0$. The Schwinger functional then is proportional to the *vacuum-persistence amplitude*, the probability amplitude for recovering a system, which has initially been in the vacuum state $|\Omega\rangle$ for $T \to -\infty$, in this state for $T \to \infty$ in presence of the source J. Moreover, the Schwinger functional represents the generating functional for all n-point correlators. Closely related to the Schwinger functional is the generating functional of the connected Green's functions $E[J]$, which is defined by

$$e^{-iE[J]} := Z[J]. \tag{2.2}$$

To introduce the effective action we need to define one further quantity, the *classical field* ϕ_{cl}, which is the vacuum expectation value of the field:

$$\phi_{\text{cl}} := \langle \Omega | \phi | \Omega \rangle_J. \tag{2.3}$$

The effective action Γ is a functional of ϕ_{cl}, obtained by a Legendre transform of the generating functional $E[J]$:

$$\Gamma[\phi_{\mathrm{cl}}] := -E[J] - \int d^4y \; J(y)\phi_{\mathrm{cl}}(y). \tag{2.4}$$

In the language of Feynman's diagrammar, $\Gamma[\phi_{\mathrm{cl}}]$ is the generating functional of 1PI Green's functions, also called proper vertices.

2.1.2 Euclidean Space

The Euclidean effective action Γ_{E} is $-i$ times the continuation of Γ to $-iT$, keeping in mind that T goes to infinity in the end:

$$\begin{aligned}
\Gamma_{\mathrm{E}}(T) &:= -i\Gamma(-iT) && (2.5)\\
&= iE(-iT) + i\int_{iT/2}^{-iT/2} dy^0 \int d^3y \; J(y)\phi_{cl}(y) && (2.6)\\
&\overset{y_4:=iy^0}{=} -E_{\mathrm{E}} + \int_{-T/2}^{T/2} dy_4 \int d^3y \; J(y)\phi_{cl}(y)). && (2.7)
\end{aligned}$$

We have defined the Euclidean generating functional E_{E} analogously to the Euclidean effective action, $E_{\mathrm{E}} := -iE_{\mathrm{M}}(-iT)$. That means

$$\begin{aligned}
e^{E_{\mathrm{E}}} &= \int \mathcal{D}\phi \; e^{i\int_{iT/2}^{-iT/2} dx^0 \int d^3x \; (\mathcal{L}[\phi]+J\phi)} && (2.8)\\
&\overset{\mathcal{L}_{\mathrm{E}}:=-\mathcal{L}}{=} \int \mathcal{D}\phi \; e^{-\int_{-T/2}^{T/2} dx_4 \int d^3x \; (\mathcal{L}_{\mathrm{E}}[\phi]-J\phi)} && (2.9)\\
&\overset{S_{\mathrm{E}}:=\int dx_{\mathrm{E}} \; \mathcal{L}_{\mathrm{E}}}{=} \int \mathcal{D}\phi \; e^{-S_{\mathrm{E}}[\phi]+\int dx_{\mathrm{E}} \; J\phi}. && (2.10)
\end{aligned}$$

Throughout this thesis we will work in Euclidean spacetime, if not stated otherwise, but physical external fields will be kept Minkowski-valued. To avoid cluttering up the notation, we will drop the subscript E in the following.

2.2 1-Loop Computation of the Effective Action

We evaluate the path integral in (2.10) with the steepest-descent approximation. ϕ_{s} denotes the stationary point of the exponent, i.e.,

$$\frac{\delta}{\delta\phi(x)}\left(S[\phi] - \int dy \; J\phi\right)\Big|_{\phi_{\mathrm{s}}} = 0 \tag{2.11}$$

for all x. Expanding the exponent about $\phi_{\rm s}$ with the notation $\eta := \phi - \phi_{\rm s}$ yields

$$\begin{aligned} S[\phi] - \int dx\ J\phi &= S[\phi_{\rm s}] - \int dx\ J\phi_{\rm s} \\ &\quad + \int dx\ \eta(x) \left(\left. \frac{\delta S[\tilde{\phi}]}{\delta\tilde{\phi}(x)} \right|_{\phi_{\rm s}} - J(x) \right) \\ &\quad + \frac{1}{2} \int dx \int dy\ \eta(x)\ \left. \frac{\delta^2 S[\tilde{\phi}]}{\delta\tilde{\phi}(x)\delta\tilde{\phi}(y)} \right|_{\phi_{\rm s}} \eta(y) \\ &\quad + \cdots . \end{aligned} \tag{2.12}$$

The second term on the right-hand side is zero because of (2.11). Thus

$$\begin{aligned} e^E &\approx e^{-S[\phi_{\rm s}] + \int dx\ J\phi_{\rm s}} \int \mathcal{D}\eta\ e^{-\frac{1}{2}\int dx \int dy\ \eta(x) \left. \frac{\delta^2 S[\tilde{\phi}]}{\delta\tilde{\phi}(x)\delta\tilde{\phi}(y)} \right|_{\phi_{\rm s}} \eta(y)} \\ &= \mathcal{N} e^{-S[\phi_{\rm s}] + \int dx\ J\phi_{\rm s}} {\rm Det}^{-\frac{1}{2}} \left. \frac{\delta^2 S}{\delta\phi\delta\phi} \right|_{\phi_{\rm s}} . \end{aligned} \tag{2.13}$$

For the generating functional we get

$$E[J] \approx -S[\phi_{\rm s}] + \int dx\ J\phi_{\rm s} - \frac{1}{2} {\rm Tr} \ln \left. \frac{\delta^2 S}{\delta\phi\delta\phi} \right|_{\phi_{\rm s}} , \tag{2.14}$$

dropping the constant term $\ln \mathcal{N}$. The effective action now reads

$$\Gamma \approx S[\phi_{\rm s}] + \frac{1}{2} {\rm Tr} \ln \left. \frac{\delta^2 S}{\delta\phi\delta\phi} \right|_{\phi_{\rm s}} . \tag{2.15}$$

The classical field is just $\delta E/\delta J$. Consequently, by using only the leading order of (2.14),

$$\phi_{cl} \approx \frac{\delta}{\delta\phi_{\rm s}} (-S[\phi_{\rm s}] + \int dx\ J\phi_{\rm s}) \frac{\delta\phi_{\rm s}}{\delta J} + \phi_{\rm s} = \phi_{\rm s} \tag{2.16}$$

due to (2.11). Hence we can write, to first order,

$$\Gamma \approx S[\phi_{cl}] + \frac{1}{2} {\rm Tr} \ln \left. \frac{\delta^2 S}{\delta\phi\delta\phi} \right|_{\phi_{\rm cl}} . \tag{2.17}$$

We have obtained this result for real fields. For fields with more than one degree of freedom we get additional combinatorial factors. In case of a complex field, for example, we get

$$\Gamma \approx S[\phi_{cl}] + {\rm Tr} \ln \left. \frac{\delta^2 S}{\delta\phi^*\delta\phi} \right|_{\phi_{\rm cl}} . \tag{2.18}$$

This expression is of central interest in the present work. The effective action governs the dynamics of the VEV of the field. In the present approximation, it is given by the classical action plus corrections due to the quantum fluctuations in Gaußian approximation.

The steepest-descent approximation is valid for large exponents in (2.10), that is if the classical action is large compared to the quantum of action $\hbar$, which is equal to one in natural units. In fact the approximation we have used is an expansion in $\hbar$ up to $\mathcal{O}(\hbar)$ as can be shown by explicitly tracing $\hbar$ throughout the calculation. This in turn is equivalent to a loop expansion up to one-loop order. We emphasize that we have not performed a coupling expansion, expression (2.10) contains tree and one-loop diagrams to all orders in the coupling times the classical field.

Despite the plain structure of (2.18), evaluating the functional trace in general poses a great challenge. Exact analytical treatment using the generalized zeta function [40] or Schwinger's propertime approach [4] requires the knowledge of the spectrum of $\frac{\delta^2 S}{\delta\phi\delta\phi}$. In QED this is known, for instance, for the case of a constant pure magnetic field, which will be studied analytically in section 2.8.1, and more generally for a uniform, but otherwise arbitrary, electromagnetic background (Heisenberg-Euler action [2, 3, 41]). For inhomogeneous fields, in the majority of cases, one is reliant on approximations. If the background varies slowly with respect to the Compton wavelength $1/m$, regarding the field as locally constant and using the Euler-Heisenberg result is a valid approximation. Beyond this approximation one can perform a derivative expansion, still facing restrictions on the field variation. Up to now, also standard numerical methods rely on highly symmetric background fields or use spacetime discretization.

In this thesis a new numerical algorithm is developed to evaluate the imaginary part of the functional trace for inhomogeneous background fields. We bypass the difficulties of prior approaches by applying an emerging technique called *worldline numerics* which combines the string-inspired *worldline formalism* with Monte Carlo methods.

2.3 Worldline Representation of the Effective Action

Let us now present the basis of the announced numerical algorithm, the so-called *worldline formalism*. This formalism will result in an analytical expression for the functional trace in (2.17), which is not only predestinated for numerical implementation, but moreover has a nice physical interpretation giving some qualitative understanding of the effective action's nonlocal character.

To make expressions more concise we define

$$H_{\mathrm{w}} := \frac{\delta^2 S}{\delta\phi\delta\phi}. \tag{2.19}$$

The first-order correction to the effective action, i.e., the second term of (2.18), we call Γ^1.

In the first step towards the worldline formalism we switch to Schwinger's propertime representation, using Frullani's integral,

$$\Gamma^1 := \mathrm{Tr}\ln H_{\mathrm{w}} = -\int_0^\infty \frac{dT}{T}\mathrm{Tr}(e^{-H_{\mathrm{w}}T} - e^{-T}).$$

The second term in the trace is field independent an thus dropped in the following. We perform the functional trace in x-space.

$$\Gamma^1 = -\int_0^\infty \frac{dT}{T}\int dx\langle x|e^{-H_{\mathrm{w}}T}|x\rangle \tag{2.20}$$

Now we make the second and essential step: The matrix element $\langle x|e^{-H_{\mathrm{w}}T}|x\rangle$ can be treated analogously to transition amplitudes in quantum mechanics, where we write matrix elements as path integrals:

$$\langle x_2|e^{-iHT}|x_1\rangle = \mathcal{N}\int_{\substack{x(0)=x_1\\x(T)=x_2}} \mathcal{D}x(t)\ e^{i\int_0^T dt\ L}. \tag{2.21}$$

Hence we can write

$$\langle x|e^{-H_{\mathrm{w}}T}|x\rangle \quad = \quad \mathcal{N}\int_{x(0)=x(-iT)=x} \mathcal{D}x(t)\ e^{i\int_0^{-iT} dt\ L_{\mathrm{w}}} \tag{2.22}$$

$$\overset{\tau:=it}{=} \quad \mathcal{N}\int_{x(0)=x(T)=x} \mathcal{D}x(\tau)\ e^{\int_0^T d\tau\ L_{\mathrm{w}}}, \tag{2.23}$$

where $L_{\rm w}$ is the *worldline Lagrangian* corresponding to the *worldline Hamiltonian* $H_{\rm w}$ in (2.19). To sum up,

$$\begin{aligned}\Gamma^1 &= -\int_0^\infty \frac{dT}{T}\int dx\,\mathcal{N}\int_{x(0)=x(T)=x}\mathcal{D}x(\tau)\;e^{\int_0^T d\tau\;L_{\rm w}}\\ &= -\int_0^\infty \frac{dT}{T}\,\mathcal{N}\int_{x(0)=x(T)}\mathcal{D}x(\tau)\;e^{\int_0^T d\tau\;L_{\rm w}}.\end{aligned}\tag{2.24}$$

This is the one-loop contribution to the effective action in the so-called *worldline representation*. Having started with a D-dimensional field theory, we conclude with an expression containing a field $x(\tau)$ in one dimension, but with D components. We have mapped the set of quantum fluctuations on top of a given background to an ensemble of closed worldlines that can be interpreted as the traces of the quantum fluctuations in spacetime. Each trace gathers information about the background along the worldline. For an even more visual interpretation we need to know $L_{\rm w}$, which is derived for scalar QED in the next section.

2.4 Worldline Formalism in Scalar QED

We will now compute $L_{\rm w}$ in (2.24) for scalar QED. The Euclidean Lagrangian of the field theory reads

$$\mathcal{L} = \frac{1}{4}F_{\mu\nu}^2 + (D_\mu\phi)^* D_\mu\phi + m^2\phi^*\phi,\tag{2.25}$$

with $D_\mu = \partial_\mu + ieA_\mu$. H_w acting on an arbitrary field η yields:

$$\begin{aligned}(H_{\rm w}\eta)(x) &= \int dy\frac{\delta^2 S}{\delta\phi^*(x)\delta\phi(y)}\eta(y)\\ &= \int dy\frac{\delta^2}{\delta\phi^*(x)\delta\phi(y)}\int dz\\ &\quad\left(\frac{1}{4}F_{\mu\nu}^2 + ((\partial_z - ieA(z))\phi^*(y))((\partial_z + ieA(z))\phi(z)) + m^2\phi^*\phi\right)\eta(y)\\ &= \int dy\frac{\delta}{\delta\phi^*(x)}\left((-\partial_y + ieA(y))(\partial_y - ieA(y))\phi^*(y) + m^2\phi^*(y)\right)\eta(y)\\ &= \left(-(\partial_x + ieA(x))^2 + m^2\right)\eta(x),\end{aligned}\tag{2.26}$$

and we can formally write

$$H_{\rm w} = -(\partial + ieA)^2 + m^2.\tag{2.27}$$

The corresponding Lagrangian is

$$L_{\rm w} = \frac{1}{4}\dot{x}^2 - e\dot{x}A(x) - m^2, \tag{2.28}$$

as can be checked easily by a Legendre transform. In (2.24) the integration variable is $\tau = it$, thus it is useful to substitute the t derivatives by τ derivatives which are denoted by the dot from now on, $\frac{d}{dt}x = i\frac{d}{d\tau}x =: i\dot{x}$. Now, the worldline representation of the first-order contribution to the effective action in scalar QED reads

$$\Gamma^1 = -\int_0^\infty \frac{dT}{T}\,\mathcal{N}\int_{x(0)=x(T)} \mathcal{D}x(\tau)\; e^{-\int_0^T d\tau\,\left(\frac{\dot{x}^2}{4}+ie\dot{x}A(x)+m^2\right)}. \tag{2.29}$$

We can split the path integral into an ordinary integral over all x_0 and a path integral over all paths with centre of mass x_0.

$$\Gamma^1 = -\int_0^\infty \frac{dT}{T}\int dx_0\,\mathcal{N}\int_{\substack{x(0)=x(T)\\ \text{CM } x_0}} \mathcal{D}x(\tau)\; e^{-\int_0^T d\tau\,\left(\frac{\dot{x}^2}{4}+ie\dot{x}A(x)+m^2\right)}. \tag{2.30}$$

The normalization $\mathcal{N}$ is determined from the limit of zero potential, for which the diagonal elements in (2.20) can be computed analytically.

$$\begin{aligned}
\Gamma^1\big|_{A=0} &= -\int_0^\infty \frac{dT}{T}\int dx \langle x|e^{-(-\partial^2+m^2)T}|x\rangle \\
&= -\int_0^\infty \frac{dT}{T}\int dx \frac{1}{(4\pi T)^{D/2}} e^{-m^2T} \\
&= -\int_0^\infty \frac{dT}{T}\int dx_0\,\mathcal{N}\int_{\substack{x(0)=x(T)\\ \text{CM } x_0}} \mathcal{D}x(\tau)\; e^{-\int_0^T d\tau\,\left(\frac{\dot{x}^2}{4}+m^2\right)} \\
\Longrightarrow \qquad \mathcal{N} &= \frac{1}{(4\pi T)^{D/2}}\,\frac{1}{\int_{\substack{x(0)=x(T)\\ \text{CM } x_0}} \mathcal{D}x(\tau) e^{-\int_0^T d\tau\;\frac{\dot{x}^2}{4}}}.
\end{aligned} \tag{2.31}$$

Defining the *Wilson loop*

$$W := e^{-ie\int_0^T d\tau\;\dot{x}A(x)} \tag{2.32}$$

and its *expectation value*

$$\langle W\rangle := \frac{\int_{\substack{x(0)=x(T)\\ \text{CM } x_0}} \mathcal{D}x(\tau)\; W e^{-\int_0^T d\tau\;\frac{\dot{x}^2}{4}}}{\int_{\substack{x(0)=x(T)\\ \text{CM } x_0}} \mathcal{D}x(\tau) e^{-\int_0^T d\tau\;\frac{\dot{x}^2}{4}}}, \tag{2.33}$$

we can write

$$\Gamma^1 = -\frac{1}{(4\pi)^{D/2}} \int dx_0 \int_0^\infty \frac{dT}{T^{D/2+1}} e^{-m^2 T} \langle W \rangle. \tag{2.34}$$

It can be useful to split W into a symmetric and an antisymmetric part,

$$\begin{aligned} W &= \cos\left(e\int_0^T d\tau\ \dot{x}A(x)\right) \\ &\quad -i\sin\left(e\int_0^T d\tau\ \dot{x}A(x)\right). \end{aligned} \tag{2.35}$$

For any path $x(\tau)$ with Wilson loop value W, the path $x^-(\tau) := x(1-\tau)$ has the same weight $e^{-\int_0^T d\tau \frac{\dot{x}^2}{4}}$, but Wilson loop value W^{-1}. This leads to a cancellation of the sin part in (2.35) when performing the path integral. This is not surprising, as it is antisymmetric in the field strength. Thus, for further calculations, only the *cos* part is needed to which W_e refers from now on:

$$W_\mathrm{e} := \cos\left(e\int_0^T d\tau\ \dot{x}A(x)\right). \tag{2.36}$$

The exponential term in the denominator of (2.33) damps the contribution of paths with large proper length to the path integral. Hence the Wilson loop expectation value $\langle W \rangle$ at x_0 is dominated by paths with small proper length, which are somehow close to their centre of mass x_0. This leads to the following interpretation of (2.34): Around each point x_0 in space-time there is an accumulation of closed worldlines which we call *loop cloud* in the following. The role of the parameter T becomes more clear by the introduction of the *unit loop* $y(t)$, which is also most convenient for the numerical realization. We define

$$y(t) := \frac{1}{\sqrt{T}} x(Tt) - x_0. \tag{2.37}$$

The Wilson loop expectation value then reads

$$\langle W \rangle := \frac{\int_{\substack{y(0)=y(1)\\ \mathrm{CM}\ x_0}} \mathcal{D}y(t)\ W e^{-\int_0^1 dt\ \frac{\dot{y}^2}{4}}}{\int_{\substack{y(0)=y(1)\\ \mathrm{CM}\ x_0}} \mathcal{D}y(t) e^{-\int_0^1 dt\ \frac{\dot{y}^2}{4}}}. \tag{2.38}$$

The weight factor is now independent of T, whereas the Wilson loop reads

$$W = e^{-ie\int_0^1 dt\ \sqrt{T}\dot{y}A\left(\sqrt{T}y + x_0\right)}. \tag{2.39}$$

Thus T controls the extension of the loop cloud. A small T value means a small loop cloud, whereas for large T values the cloud becomes bloated. According to the scale of the loop cloud, it picks up small-scale, i.e. UV information or large-scale (IR) information of the background field, as illustrated in Fig. 2.1. Consequently we can continuously zoom in or out of the background field by varying T. The effective action contains informations of all scales because of the T integral in Eq. (2.34).

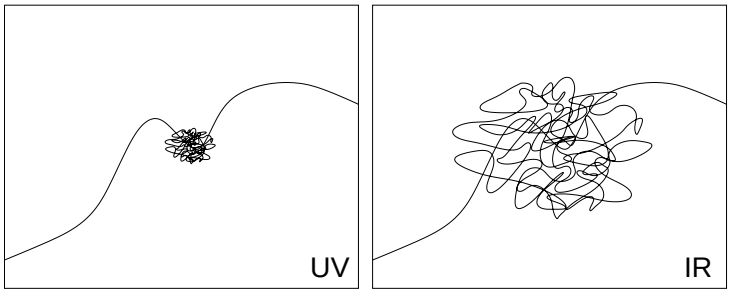

Figure 2.1: For small T values, the loop cloud gathers small-scale (UV) information of the background field, if T is increased and the cloud bloated, it picks up large scale (IR) information.

The Wilson loop expectation value at x_0 contains information about the background field gathered by the loop cloud in the neighbourhood of x_0. By this, the information is assigned to x_0 in a canonical way and, omitting the x_0 integration in (2.34), we obtain an effective action density.

2.5 Renormalization

Expression (2.34) is still formulated in unrenormalized quantities and we expect the T integrand to be divergent for $T \to 0$ due to the factor $T^{-D/2-1}$. Thus we regularize by replacing the lower bound of the T integration by a finite value Λ^{-2}. This corresponds to a UV cutoff, since the insertion of (2.27) into (2.20) leads to the term $e^{-T\partial^2}$ which damps large momenta in the trace, except for the limit $T \to 0$. Having a closer look at the Wilson loop expectation value, a heat-kernel expansion yields

$$\langle W \rangle = 1 - \frac{1}{12} T^2 e^2 F_{\mu\nu}^2(x_0) + \mathcal{O}(T^4). \tag{2.40}$$

The leading order is field independent and can therefore be dropped. As a consequence, with $D = 4$, the next order $\propto T^2$ is the only one leading to a

divergence and therefore is integrated separately:

$$\begin{aligned}\Gamma^1 &= -\frac{1}{(4\pi)^2}\int_0^\infty \frac{dT}{T^3}e^{-m^2T}\int dx_0\left(\langle W\rangle - 1 + \frac{1}{12}T^2e^2F_{\mu\nu}^2(x_0)\right)\\ &\quad +\frac{1}{(4\pi)^2}\int_{\Lambda^{-2}}^\infty \frac{dT}{T^3}e^{-m^2T}\int dx_0\ \frac{1}{12}T^2e^2F_{\mu\nu}^2(x_0)\end{aligned} \tag{2.41}$$

In the first line, we have already replaced the lower bound by 0, since the integral is finite. In the second line, the T integration can be performed analytically and this line becomes

$$\begin{aligned}&\tfrac{1}{192\pi^2}\mathrm{Ei}(-\tfrac{m^2}{\Lambda^2})\int dx_0\ e^2F_{\mu\nu}^2(x_0)\\ =\ &\tfrac{1}{192\pi^2}\left(C-\ln(\tfrac{\Lambda^2}{m^2})\right)\int dx\ e^2F_{\mu\nu}^2(x_0)+\mathcal{O}(\tfrac{m^2}{\Lambda^2}),\end{aligned} \tag{2.42}$$

where C denotes Euler's constant $C \approx 0.577216$. Together with the bare Maxwell action, the complete effective action to first order now reads

$$\begin{aligned}\Gamma &= \int dx_0\left(\frac{1}{4}\left(1-\frac{e^2}{48\pi^2}\left(C-\ln\frac{\Lambda^2}{m^2}\right)\right)F_{\mu\nu}^2+(D_\mu\phi_{cl})^*D_\mu\phi_{cl}+m^2\phi_{cl}^*\phi_{cl}\right)\\ &\quad -\frac{1}{(4\pi)^2}\int_0^\infty\frac{dT}{T^3}e^{-m^2T}\int dx_0\left(\langle W\rangle-1+\frac{1}{12}T^2e^2F_{\mu\nu}^2\right)+\mathcal{O}(\frac{m^2}{\Lambda^2}),\end{aligned} \tag{2.43}$$

where e and F denote the bare coupling and field. We impose the renormalization condition

$$\frac{\partial\Gamma}{\partial\frac{1}{4}F_{\mathrm{R}}^2}=1-\frac{e_{\mathrm{R}}^2}{48\pi^2}\ln\frac{m^2}{\mu^2}, \tag{2.44}$$

ensuring that the photon propagator is canonically normalized for electron on-shell renormalization conditions $\mu = m$. The renormalized field is connected to the bare one via

$$F_{\mathrm{R}}^2 = Z_{\mathrm{F}}F^2 \tag{2.45}$$

with

$$Z_{\mathrm{F}} = 1-\frac{e^2}{48\pi^2}\left(C-\ln\frac{\Lambda^2}{\mu^2}\right), \tag{2.46}$$

whereas the renormalized charge satisfies

$$e_{\mathrm{R}}^2 = Z_{\mathrm{F}}^{-1}e^2, \tag{2.47}$$

such that $eF = e_{\rm R}F_{\rm R}$ remains invariant. We rediscover the β-function for scalar QED, $\beta(e_{\rm R}^2) = \mu\partial_\mu e_{\rm R}^2(\mu) = e_{\rm R}^4/(24\pi^2)$. Inserting (2.45) into (2.43) and imposing the electron on-shell condition $\mu = m$, the first line reads

$$\int dx_0 \left(\frac{1}{4} F_{\mu\nu}^2 + (D_\mu \phi_{cl})^* D_\mu \phi_{cl} + m^2 \phi_{cl}^* \phi_{cl} \right), \tag{2.48}$$

where we have dropped the subscript R of the renormalized quantities, since we will use no bare quantities from now on. After performing the limit $\Lambda \to \infty$, the second line of (2.43) yields the renormalized one-loop contribution to the effective action,

$$\Gamma^1 = -\frac{1}{(4\pi)^2} \int_0^\infty \frac{dT}{T^3} e^{-m^2 T} \int dx_0 \left(\langle W \rangle - 1 + \frac{1}{12} T^2 e^2 F_{\mu\nu}^2(x_0) \right). \tag{2.49}$$

The divergent term of the one-loop contribution Γ^1 has been absorbed into the bare Maxwell term of the classical action and Γ^1 is UV and IR finite now. It describes the quantum corrections to Maxwell's classical electrodynamics. These corrections are non-linear in the electromagnetic field. The principle of linear superposition known from the classical theory does no longer hold. Besides, as illustrated best by the loop-cloud interpretation, this leads to a non-local effective theory.

2.6 Worldline Formalism in Spinor QED

In spinor QED, instead of the plus in Eq. (2.18), one obtains a minus, due to the Grassmann properties of the field. The Lagrangian in Euclidean space reads

$$\mathcal{L} = \frac{1}{4} F_{\mu\nu}^2 + \bar{\psi} i \not{D} \psi + m \bar{\psi} \psi \tag{2.50}$$

and the functional derivation of the corresponding action yields

$$\frac{\delta^2 S}{\delta \bar{\psi} \delta \psi} = i \not{D} + m. \tag{2.51}$$

Thus the one-loop order of the effective action reads

$$\Gamma^1_{\rm spinor} = -\ln \mathrm{Det}(i \not{D} + m). \tag{2.52}$$

In four dimensions the effective action is a Lorentz scalar and consequently independent of the sign of $\not{D}$. Hence we can write

$$\begin{aligned} \mathrm{Det}(i\not{D}+m) &= \mathrm{Det}(-i\not{D}+m) \\ &= (\mathrm{Det}(i\not{D}+m)\mathrm{Det}(-i\not{D}+m))^{\frac{1}{2}} \\ &= \mathrm{Det}^{\frac{1}{2}}\left(\not{D}^2+m^2\right) \end{aligned} \tag{2.53}$$

and we obtain

$$\begin{aligned} \Gamma^1_{\text{spinor}} &= -\frac{1}{2}\mathrm{Tr}\ln\left(\not{D}^2+m^2\right) \\ &= -\frac{1}{2}\mathrm{Tr}\ln\left(-(\partial+ieA)^2+m^2-i\frac{1}{2}e\sigma^{\mu\nu}F_{\mu\nu}\right), \end{aligned} \tag{2.54}$$

where $\sigma^{\mu\nu}$ denotes $\frac{1}{2}[\gamma^\mu,\gamma^\nu]$. The argument of the logarithm corresponds to H_{w} in Eq. (2.27) of the preceding section. The only difference is the additional spinor term $-i\frac{1}{2}e\sigma^{\mu\nu}F_{\mu\nu}$. Consequently the worldline Lagrangian Eq. (2.28) now reads

$$L_{\text{w}} = \frac{1}{4}\dot{x}^2 - e\dot{x}A(x) - m^2 + i\frac{1}{2}e\sigma^{\mu\nu}F_{\mu\nu}, \tag{2.55}$$

and we end up with the "spinorial Wilson loop"

$$W_{\text{spinor}} = e^{-ie\int_0^T d\tau\ \dot{x}A(x)}\ \mathrm{tr}_\gamma P e^{ie\int_0^T d\tau\ \frac{1}{2}\sigma^{\mu\nu}F_{\mu\nu}(x)}, \tag{2.56}$$

where tr_γ denotes the spinor part of the functional trace in Eq. (2.54). By introducing $\bar{F}_{\mu\nu} := \frac{1}{T}\int_0^T F_{\mu\nu}(x)$ we can write

$$W_{\text{spinor}} = e^{-ie\int_0^T d\tau\ \dot{x}A(x)}\ \mathrm{tr}_\gamma P e^{iTe\frac{1}{2}\sigma^{\mu\nu}\bar{F}_{\mu\nu}}. \tag{2.57}$$

The one-loop contribution to the effective action in spinor QED is then given by

$$\Gamma^1_{\text{spinor}} = \frac{1}{2}\frac{1}{(4\pi)^{D/2}}\int dx_0 \int_0^\infty \frac{dT}{T^{D/2+1}} e^{-m^2T}\langle W_{\text{spinor}}\rangle. \tag{2.58}$$

We resume that the one-loop contribution to the effective action in spinor QED differs from the scalar QED result Eq. (2.34) in an additional spinor term in the Wilson loop and an overall factor $-\frac{1}{2}$. Analogously to renormalization in scalar QED, one obtains the renormalized expression

$$\Gamma^1_{\text{spinor}} = \frac{1}{2}\frac{1}{(4\pi)^{D/2}}\int dx_0 \int_0^\infty \frac{dT}{T^{D/2+1}} e^{-m^2T}\left(\langle W_{\text{spinor}}\rangle - 1 - \frac{1}{6}T^2e^2F^2_{\mu\nu}(x_0)\right), \tag{2.59}$$

which is closely related to the scalar-QED expression Eq. (2.49).

2.7 Worldline Numerics in Scalar QED

As announced, expression (2.49) is predestinated for numerical computation. Paths of large proper length are suppressed in the Wilson loop expectation value (2.33) by the kinetic term of the worldline $\propto \dot{y}^2$, which has already led us to the introduction of the term *loop cloud* and makes it possible to approximate the path integrals by sums over finite path ensembles. For an ensemble of paths that are distributed according to the exponential weight factor $\exp(-\int_0^1 d\tau\ \frac{\dot{y}^2}{4})$, the Wilson loop expectation value is equal to the ensemble average of W. For the numerical implementation, we need to discretise the loops, that means each loop $y(t)$ is represented by a finite number of N supporting points y_k at $t = k/N$ with $k = 1, \cdots, N$,

$$y(t) \to \{y_k\} := \{y(\frac{k}{N})\}. \tag{2.60}$$

We use the *vloop* algorithm to create an ensemble of n_{L} discrete and closed unit loops $\{y_k\}$ with the distribution functional

$$P[\{y_k\}] = \delta(y_1 + \cdots + y_N) \exp\left(-\frac{N}{4}\sum_{k=1}^{N}(y_k - y_{k-1})^2\right). \tag{2.61}$$

This is the discrete form of the weight factor $\exp(-\int_0^1 d\tau\ \frac{\dot{y}^2}{4})$, the delta function reflects the fact, that only *closed* loops are generated. The vloop algorithm is reviewed in appendix A.1. Once the loop ensemble has been generated, it can be used to compute $\langle W \rangle$ for different T and x_0.

First W is computed for each unit loop. It is tempting to interpret the supporting points as defining a polygon and perform the t integral in (2.39) analytically. With regard to the Wilson loop, this is advantageous, since it conserves gauge invariance. Nevertheless, the polynomial interpolation distorts the loop ensemble, it does not preserve the desired spacial information. The interpolated paths have a smaller average distance to the centre of mass x_0 than their supporting points, thus interpolation actually means shrinking the loop cloud. The background field is no longer scanned in the desired range. For small N this effect leads to results with a sizeable systematic error. Hence, we make a simple step-function approximation:

$$\int_0^1 dt \dot{y} A(\sqrt{T}y + x_0) \approx \sum_{k=1}^{N}(y_{k+1} - y_k) A(\sqrt{T}y_k + x_0), \tag{2.62}$$

where we have used $\dot{y} = N(y_{k+1} - y_k)$. The potential A is evaluated only at the points y_k, we do not make any further assumptions about the path in between. As a side effect, simpler mathematical expressions arise which lead to a significantly faster numerical evaluation.

After W has been computed for each loop, we merely have to take the average to obtain the Wilson loop expectation value,

$$\langle W \rangle = \frac{1}{n_{\mathrm{L}}} \sum_{\{y\}} W[y]. \tag{2.63}$$

The standard error provides an estimate of the statistical error,

$$\Delta\langle W \rangle = \frac{1}{\sqrt{n}_L} \sqrt{\langle W^2 \rangle - \langle W \rangle^2}. \tag{2.64}$$

In addition to this statistical error the discreteness of the loops leads to a systematic error. The number of supporting points N has to be chosen sufficiently large, such that this error can be neglected compared to the statistical error. In practice, the value to choose depends on the background field. N should be adjusted, so that the distance $|x_{k+1} - x_k| = \sqrt{T}|y_{k+1} - y_k|$ is smaller than the characteristic length scale of the inhomogeneities of the field for most loops and k. For large N, the distance is distributed according to the weight $\exp(-N/(4T)(|x_{k+1} - x_k|)^2)$ with the standard deviation $\sigma = \sqrt{\frac{2T}{N}}$. Comparison of σ to the length scale of the background field helps us to make a reasonable choice for N.

To summarize, the numerical estimate is governed by two parameters, n_{L} and N. Each controls one of the two approximations we have made so far: Both the path integral and the loop propertime integral have been replaced by a finite sum. It is noteworthy, that we have *not* discretized space-time.

2.8 Example: Constant Magnetic Field

2.8.1 Analytic Calculation

Let us examine the case of a constant B field in x^1 direction given by $A_{\mathrm{M}} = (0, 0, 0, Bx^2)^\top$ in Minkowski space. In Euclidean space the potential A, as used in the previous sections, is defined by $A_4 = iA^0_{\mathrm{M}}$ and $A_j = A^j_{\mathrm{M}}$, $j = 1, \cdots, 3$. Hence the constant B field is given by $A = (0, 0, Bx_2, 0)^\top$ and $F_{\mu\nu}$

reads

$$F_{\mu\nu} = \begin{pmatrix} 0 & 0 & 0 & 0 \\ 0 & 0 & -B & 0 \\ 0 & B & 0 & 0 \\ 0 & 0 & 0 & 0 \end{pmatrix}. \tag{2.65}$$

Expression (2.20) is the starting point of our calculation. Inserting H_w for scalar QED (2.27) yields

$$\Gamma^1 = -\int_0^\infty \frac{dT}{T} e^{-m^2 T} \mathrm{Tr}\ e^{T(\partial + ieA)^2}. \tag{2.66}$$

The operator $(\partial + ieA)^2 = \partial^2 + i2eBx_2\partial_3 - e^2B^2x_2^2$ has the eigenstates

$$e^{-i(k_1x_1 + k_3x_3 + k_4x_4)} \psi_n(x_2 - \frac{k_3}{eB}), \tag{2.67}$$

where ψ_n are eigenstates of the one dimensional harmonic oscillator,

$$(-\partial_x^2 + e^2B^2x^2)\psi_n(x) = eB(2n+1)\psi_n(x). \tag{2.68}$$

The corresponding eigenvalues are

$$-(k_1^2 + k_4^2 + eB(2n+1)). \tag{2.69}$$

We can now evaluate the trace by means of box quantization. Using a box with sides $L_1, \cdots, L_4$ and periodic boundary conditions, the sum over all eigenstates passes into

$$\int_{-\infty}^{\infty} \frac{L_1}{2\pi} dk_1 \int_0^{eBL_2} \frac{L_3}{2\pi} dk_3 \int_{-\infty}^{\infty} \frac{L_4}{2\pi} dk_4 \sum_{n=0}^{\infty}, \tag{2.70}$$

where we use integral notation, since we will finally take $L_i \to \infty$. Note the integration boundaries of the k_3-integration: Due to the periodic boundary conditions we actually do not use the eigenstates (2.67), which are not periodic. Instead of ψ_n we use the linear combination $\sum_{l=-\infty}^{\infty} \psi_n(x - \frac{k_3 + leBL_2}{eB})$, which has no effect on the eigenvalues (2.69). These linear combinations are a basis of all periodic combinations of ψ_n. Obviously they are periodic in k_3 with period eBL_2, which leads to the above mentioned integration boundaries. The trace now reads

$$\begin{aligned} \mathrm{Tr} e^{T(\partial_x + ieA(x))^2} &= \int_{-\infty}^{\infty} \frac{L_1}{2\pi} dk_1 \int_0^{eBL_2} \frac{L_3}{2\pi} dk_3 \int_{-\infty}^{\infty} \frac{L_4}{2\pi} dk_4 \sum_{n=0}^{\infty} e^{-T(k_1^2 + k_4^2 + eB(2n+1))} \\ &= \frac{L_1L_2L_3L_4}{16\pi^2T^2} \frac{TeB}{\sinh(TeB)}, \end{aligned} \tag{2.71}$$

and Γ^1

$$\Gamma^1 = -\frac{L_1L_2L_3L_4}{16\pi^2}\int_0^\infty \frac{dT}{T^3}e^{-m^2T}\frac{TeB}{\sinh(TeB)} \tag{2.72}$$

$$\stackrel{L_i\to\infty}{\longrightarrow} -\frac{1}{16\pi^2}\int_0^\infty \frac{dT}{T^3}e^{-m^2T}\int d^4x_0\frac{TeB}{\sinh(TeB)}. \tag{2.73}$$

Comparison to Eq. (2.34) yields

$$\langle W\rangle = \frac{TeB}{\sinh(TeB)}. \tag{2.74}$$

The renormalized effective action (2.49) now reads

$$\Gamma^1 = -\frac{1}{(4\pi)^2}\int_0^\infty \frac{dT}{T^3}e^{-m^2T}\int d^4x_0\left(\frac{TeB}{\sinh(TeB)} - 1 + \frac{1}{6}T^2e^2B^2\right). \tag{2.75}$$

This is the well known Heisenberg-Euler effective action of scalar QED for a homogeneous B field [2].

2.8.2 Numerical Computation

Let us now study the field configuration of the previous section with the numerical method presented in section 2.7. Equation (2.36) reads

$$W_{\rm e} = \cos(TeBI), \tag{2.76}$$

where we have introduced $I := \int_0^1 dt\ \dot{y}_3y_2$.

In Fig. 2.2 the numerical values of $\langle W\rangle = \langle W_{\rm e}\rangle$ for several values TeB are compared to the exact result (2.74) with satisfactory agreement. We have used an ensemble of $n_{\rm L} = 5000$ loops where each loop is specified by $N = 1000$ ppl (points per loop). The last number is certainly larger than necessary for a constant background field. One could safely choose only 100 supporting points, but with regard to inhomogeneous fields, where more supporting points are needed, we get a better idea of the algorithm's performance.

The computations so far are quite simple and with the chosen values for n_L and N, the algorithm is very fast, it took only some seconds CPU time on an ordinary workstation to produce Fig. 2.2. The already convincing result could be enhanced by increasing the number of loops $n_{\rm L}$. Nevertheless, for numerical renormalization, small statistical errors are not sufficient. Inserting

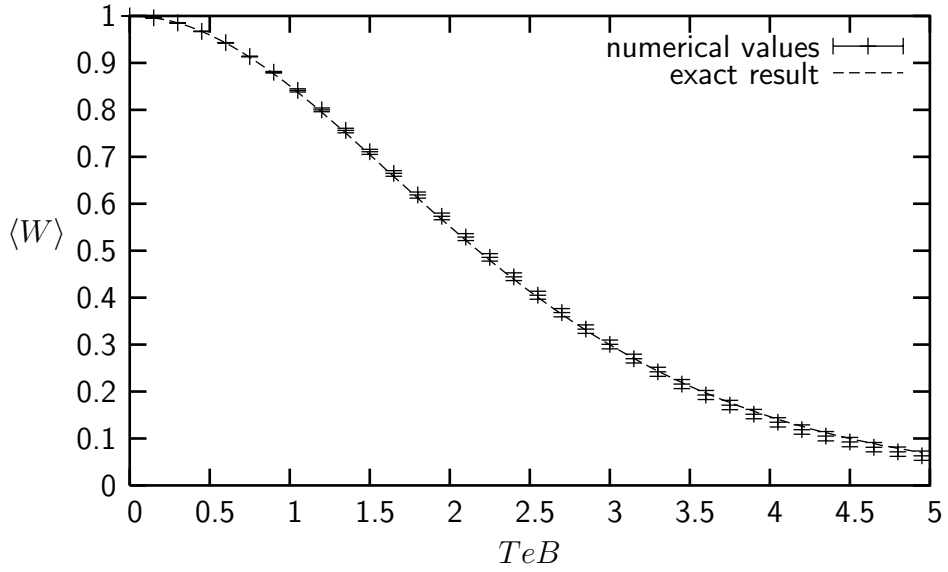

Figure 2.2: Wilson loop expectation value for a constant magnetic field: exact result equation (2.74) in comparison with the numerical estimate. Number of loops: $n_{\mathrm{L}} = 5000$. Points per loop: $N = 1000$ ppl.

this into Eq. (2.49) and omitting the x_0 integration yields the one-loop contribution to the renormalized effective Lagrangian

$$\mathcal{L}^1_{\mathrm{eff}} = -\frac{1}{(4\pi)^2}\int_0^\infty \frac{dT}{T^3} e^{-m^2 T}\left(\langle W_{\mathrm{e}}\rangle - 1 + \frac{1}{6}T^2e^2B^2\right). \tag{2.77}$$

Even the slightest deviation of the first orders of $\langle W\rangle$ from the exact result prevent the counterterms to cancel the divergencies for $T \to 0$. The first orders have to be known exactly. Fortunately we know them exactly. The counterterms have been determined by use of the heat-kernel expansion (2.40). We can use this expansion again and adjust the pure worldline numerical result. This is done by fitting a polynomial to the numerical values of $\langle W\rangle$ for small T, the first three terms of which are fixed by the expansion. The polynomial together with the fit errors then can be used instead of the previously calculated values for small T.

Figure 2.3 shows the corrected propertime integrand of Eq. (2.77) without the mass term. It vanishes for $T = 0$. Without the correction it would be divergent for $T \to 0$.

The polynomial fit has been performed with *Numerical Recipes' lfit*-function. We have used a polynomial of fourth order fitted to five values

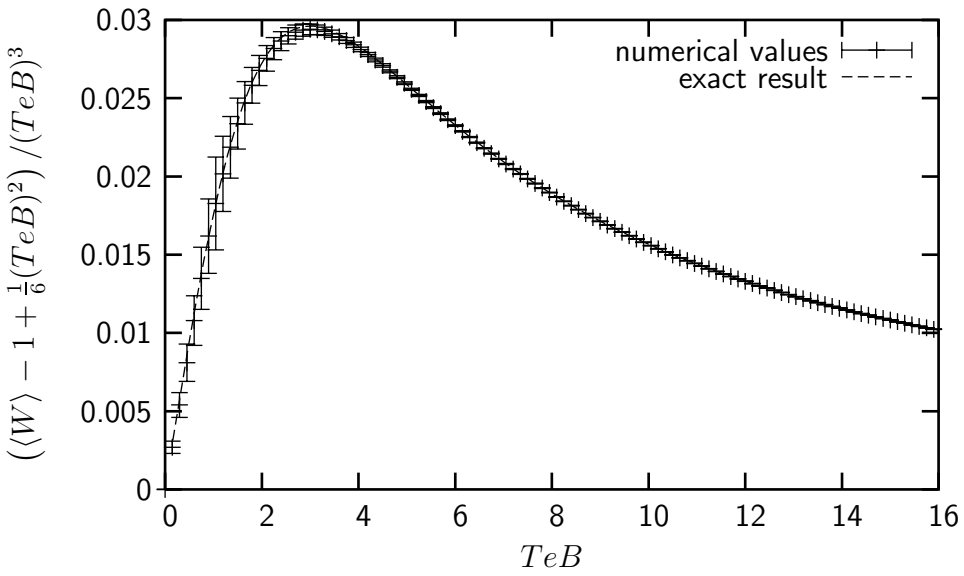

Figure 2.3: The propertime integrand in (2.77) without the mass term: exact result in comparison with the numerical estimate. $n_{\rm L} = 5000$, $N = 1000$.

of $\langle W\rangle$ between $TeB = 0$ and $TeB = 1$. *lfit* provides a covariance matrix C of the coefficients a_i. The error of a polynomial value is

$$\triangle P(T) = \triangle(a_0, \cdots, a_n)(1, \cdots, T^n)^\top = (1, \cdots, T^n)C(1, \cdots, T^n)^\top,$$

where n denotes the order of the polynomial. For small T this error is smaller than the statistical error of the worldline numerical Wilson loop expectation values, due to the information we have provided with the knowledge of the first three coefficients. The range of T in which this is the case is about the same as the one used for the fitting procedure. In particular the error vanishes for $T \to 0$. We would like to stress that this renormalization procedure would also work if we did not know the exact first few terms. In this case, we could still fit the T integrand to a polynomial and subtract the first few terms. These terms would then provide us with a numerical estimate for the β function.

As a final task the T integral has to be performed. There exist several powerful algorithms for this purpose, leading to Fig. 2.4. The error of the integral is the integrated error of the integrand. This is a very conservative estimate, since it assumes the integrand's values to be strictly correlated for different T values. But indeed there is a strong correlation, as we use the same loop cloud for all T.

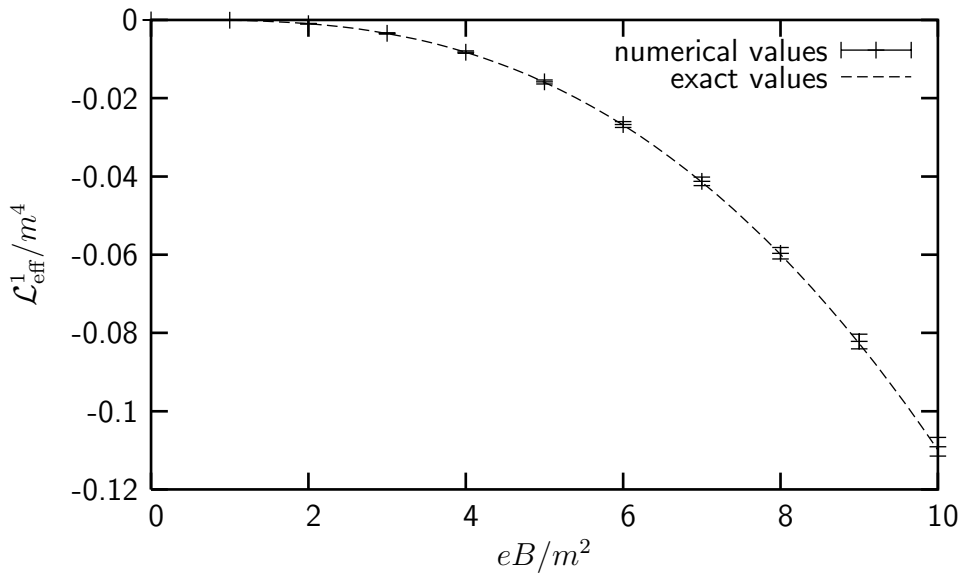

Figure 2.4: The one-loop contribution to the effective Lagrangian for the constant magnetic field: exact result in comparison with the numerical estimate. $n_L = 5000$, $N = 1000$ ppl.

We have demonstrated the successful usage of worldline numerics in scalar QED for a simple example. In the following we will develop the method further to tackle more complicated problems, in particular the electron-positron pair production in inhomogeneous electrical fields.

2.9 Worldline Numerics in spinor QED

In this thesis, we will concentrate on scalar QED, but most of the numerical computations can easily be extended to spinor QED. The essential difference to the scalar-QED computations is the extra term in the Wilson loop, cf. Eq. (2.57),

$$\mathrm{tr}_\gamma P e^{iTe\frac{1}{2}\sigma^{\mu\nu}\bar{F}_{\mu\nu}}. \tag{2.78}$$

For the example of the preceding section, the constant B field, this means no major changes for the computations. If the field is constant, for obvious reasons, the average $\bar{F}_{\mu\nu}$, and thus the complete extra term, is independent of the path. Therefore it can be factored out of the expectation value, and

the path ordering can be dropped.

$$\begin{aligned}\langle W_{\rm spinor}\rangle &= \langle e^{-ie\int_0^T d\tau\ \dot{x}A(x)}\rangle\ {\rm tr}_\gamma e^{iTe\frac{1}{2}\sigma^{\mu\nu}F_{\mu\nu}} \\ &= \langle W_{\rm scalar}\rangle\ {\rm tr}_\gamma e^{iTe\frac{1}{2}\sigma^{\mu\nu}F_{\mu\nu}}. \end{aligned} \tag{2.79}$$

With $F_{\mu\nu}$ from Eq. (2.65) we obtain

$$\sigma^{\mu\nu}F_{\mu\nu} = i2B\begin{pmatrix} 0 & 0 & 0 & 1 \\ 0 & 0 & 1 & 0 \\ 0 & 1 & 0 & 0 \\ 1 & 0 & 0 & 0 \end{pmatrix}. \tag{2.80}$$

Even powers of the matrix are equal to the identity, whereas odd powers have a vanishing trace. We can therefore write

$$\begin{aligned}\langle W_{\rm spinor}\rangle &= \langle W_{\rm scalar}\rangle\ 4\left(1+\frac{1}{2!}(TeB)^2+\frac{1}{4!}(TeB)^4+\cdots\right) \\ &= \langle W_{\rm scalar}\rangle\ 4\cosh(TeB). \end{aligned} \tag{2.81}$$

Hence, to obtain the *spinor* QED effective action for the constant B field with worldline numerics, only an analytically known extra term has to be considered when performing the T integration.

Chapter 3

Pair Production in Scalar QED

Since the early 1930's, the QED vacuum in a static spatially uniform electric background field is known to be unstable. The vacuum decays, which corresponds to the creation of particles. However, this process has not been observed experimentally ever since. This arises from the fact, that very strong electric fields are necessary to observe a sizeable production rate.

Some simple considerations lead to a first estimate for the field strength needed: Due to Heisenberg's uncertainty principle, even in the vacuum state of QED without any background field, pairs of electrons and positrons appear continously as *virtual* particles. They annihilate each other within a short amount of time due to energy conservation. An external electric field which couples to the virtual particles can lead to a *real* e^+e^- pair, by compensating for the lack of energy which arises from the newly created mass of the pair. We assume the virtual pair to have a spatial extension Δl of the same order of magnitude as the Compton wavelength of the electron, $\Delta l \approx 1/m$. The work of the field on one particle of charge e over this distance then is $eE\Delta l = eE/m$. This energy has to be equal to the mass of the particle, $eE/m \stackrel{!}{=} m$. This leads to a critical field strength $E_{\mathrm{cr}} = m^2/e \approx 1.3 \cdot 10^{16} \frac{V}{cm}$. Even if this is only a rough estimate, this numbers shows that very strong fields are necessary to observe a considerable amount of created pairs. Experimentally, these field strengths will presumably be reached on a macroscopic or mesoscopic scale with upcoming high-intensity lasers.

If the field strength is weaker than E_{cr}, pair production is not eliminated. As long as the field is able to provide the pair with enough energy to prevent it from annihilation, pair production occurs via tunneling. This is the case if the corresponding potential varies by at least $\frac{2m}{e}$. The length scale of the

variation has only a quantitative effect on the pair-production rate. If the field is weak and the variation extends over a large distance, we expect to observe less particles than for a stronger field, but if the necessary potential difference is given, pairs are produced.

An elegant approach to make quantitative predictions about pair production beyond our estimates, is the use of the effective action, as presented in the subsequent section (for details on the effective action approach in QED see [42]).

3.1 Effective Action and Pair Production

The real part of the effective action leads to vacuum polarization, the imaginary part to the pair production. To understand the latter, we make the following considerations.

In section 2.1.1, we already stated, that the vacuum-persistence amplitude is *proportional* to the Schwinger functional in Minkowski space, and thus with a suitable normalization it is *equal* to

$$Z[J] = e^{-iE_{\mathrm{M}}[J]}. \tag{3.1}$$

At $J = 0$ the generating functional $E_{\mathrm{M}}[J]$ is equal to minus the effective action, cf. Eq. (2.4), and for the vacuum persistence amplitude we obtain

$$e^{-iE_{\mathrm{M}}[0]} = e^{i\Gamma_{\mathrm{M}}[\phi_{\mathrm{cl}}|_{J=0}]}. \tag{3.2}$$

The corresponding *vacuum-persistence probability* P then is

$$P = |e^{i\Gamma_{\mathrm{M}}}|^2 = e^{-2\mathrm{Im}\Gamma_{\mathrm{M}}}. \tag{3.3}$$

That means, if the effective action has a positive imaginary part, the probability for recovering our system, which has initially been in the vacuum state for $T \to -\infty$, in the same state for $T \to \infty$, is smaller than one. This implies that the vacuum is unstable, it decays and pairs are spontaneously produced with the probability

$$1 - P = 1 - e^{-2\mathrm{Im}\Gamma_{\mathrm{M}}} > 0. \tag{3.4}$$

If the Hamiltonian H is time independent, we can write the vacuum-persistence amplitude as

$$\begin{aligned} P &= \langle\Omega|e^{-iHT}|\Omega\rangle \\ &= \langle\Omega|e^{-iH_\Omega T}|\Omega\rangle \\ &= e^{-iH_\Omega T}, \end{aligned} \tag{3.5}$$

with $T \to \infty$, where H_Ω denotes the eigenvalue of the vacuum state corresponding to H. Consequently, again for a suitable normalized Schwinger functional, we have

$$E_{\mathrm{M}} = H_\Omega T. \tag{3.6}$$

As stated in 2.1.2, the Euclidean quantity corresponding to E_{M} is defined as $E_{\mathrm{E}} = -iE_{\mathrm{M}}(-iT)$, and therefore

$$E_{\mathrm{E}} = -H_\Omega T = -E_{\mathrm{M}}. \tag{3.7}$$

In absence of sources, we reason

$$\Gamma_{\mathrm{E}} = H_\Omega T = -\Gamma_{\mathrm{M}}, \tag{3.8}$$

and for the vacuum-persistence probability we obtain

$$P = e^{2\mathrm{Im}\Gamma_{\mathrm{E}}} = e^{2\mathrm{Im}H_\Omega T}. \tag{3.9}$$

If $\mathrm{Im}\Gamma_{\mathrm{E}}$ and therewith $\mathrm{Im}H_\Omega$ is negative, this equation yields a typical exponential decay. The number of pairs created per time is equal to $2|\mathrm{Im}\Gamma_{\mathrm{E}}|/T$. Thus the production rate per space-time volume is given by twice the imaginary part of the effective Lagrangian, $2|\mathrm{Im}\mathcal{L}_{\mathrm{Eeff}}|$.

We already noted that for our conclusions a suitable normalization of the Schwinger functional is necessary. In QED the vacuum is stable if the potential A_μ is zero, consequently we demand

$$1 \stackrel{!}{=} |Z|_{A_\mu=0}|^2 = e^{2\mathrm{Im}\Gamma_{\mathrm{E}}} \tag{3.10}$$

which is equivalent to

$$\mathrm{Im}\Gamma_{\mathrm{E}}|_{A_\mu=0} \stackrel{!}{=} 0. \tag{3.11}$$

As we have seen in section 2.8, switching on a constant magnetic field has no effect on $\mathrm{Im}\Gamma_{\mathrm{E}}$. But in the presence of an electric field, the Euclidean effective action gains a negative imaginary part. In the following we will extend the use of worldline numerics to field configurations which result in effective actions with finite imaginary parts. Thereby we have to consider, that the worldline-numeric approach, as presented in prior sections, underlies principle limitations: Due to the fact, that it only includes quantum effects up to one-loop order, the Coulomb interaction between the produced particles and the resulting mass shift is neglected, as well as back-reactions of the created pairs on the external field. The external E field is partially shielded

by the created electrons and positrons and effectively becomes weaker for appropriate production rates. The possibility of considering this effect in a self-consistent approach has still to be investigated [43]. Higher-loop calculations, for instance, have shown that they indeed account for Coulomb interactions between the produced pairs [44, 45]. In addition to that we will preliminary concentrate on scalar QED, leaving the generalization to spinor QED to future investigations.

3.2 Constant Electric Field

Let us study pair production in scalar QED for the simplest electric field, the constant pure electric field. We will firstly retrieve Schwinger's analytic result before we try to implement worldline numerics straight forwardly. In doing so, we are faced with a number of problems, the analysis of which leads to a vivid understanding of the physics of pair production. During the development of an applicable worldline-numerical algorithm, we find several algorithms, each covering special cases of the general problem. One of them, the *pole fit* routine presented in section 3.2.4, will be the basis of our final universal algorithm, the *CDF fit*, which is developed in section 3.3.3. The more phenomenologically interested reader may skip the following section and continue reading chapter 3.3.

3.2.1 Analytical Approach

In section 2.8.1 we have analytically computed the Wilson loop expectation value and the effective action for a constant pure magnetic field. The case of a constant pure electric field can be deduced from this result. We know that the effective action depends on the two Lorentz invariants which characterize the electromagnetic field, $\mathcal{F} := \frac{1}{4}F^{\mu\nu}F_{\mu\nu} = \frac{1}{2}(\mathbf{B}^2 - \mathbf{E}^2)$ and $\mathcal{G} := \frac{1}{4}F^{\mu\nu}\tilde{F}_{\mu\nu} = -\mathbf{B}\cdot\mathbf{E}$. Thus we reason, for a pure E field,

$$\begin{aligned}\Gamma^1(E, B=0) &= \Gamma^1(\mathcal{F} = -\frac{1}{2}E^2, \mathcal{G} = 0) \\ &= \Gamma^1(0, B = iE). \end{aligned} \tag{3.12}$$

That means we replace B in the result (2.74) with iE to obtain $\langle W\rangle$ for the constant pure electric field:

$$\langle W\rangle = \frac{TeE}{\sin(TeE)}. \tag{3.13}$$

The significant difference to the expectation value (2.74) are the poles at $T = \frac{\pi}{eE}k$ with $k = 1, 2, \cdots$. When performing the T integral in expression (2.49), we have to choose an integration contour that avoids the poles. To obtain the desired sign of the effective action, we use a contour in the upper half plane, as shown in Fig. 3.1. The residues of the poles are real. They enter

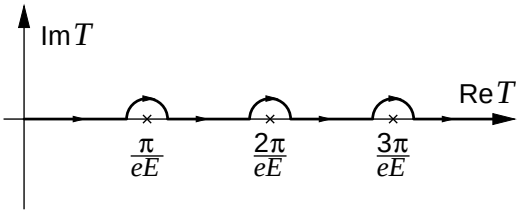

Figure 3.1: Integration contour of the T integration in Eq. (2.49) for the constant electric field.

the T integral with a purely imaginary prefactor and thus are responsible for the imaginary part of the result. In general the imaginary part of the effective action can be written as a sum over the residues:

$$\begin{aligned}
\mathrm{Im}\Gamma^1 &= \mathrm{Im}\frac{-1}{(4\pi)^2}\int dx_0 \int_0^\infty \frac{dT}{T^3} e^{-m^2 T}\left(\langle W\rangle - 1 + \frac{1}{6}\left(TeE\right)^2\right) \\
&= \frac{-1}{(4\pi)^2}\int dx_0\ \mathrm{Im}\sum_{T_{\mathrm{pol}}} \frac{1}{T_{\mathrm{pol}}^3} e^{-m^2 T_{\mathrm{pol}}}(-\pi i)\mathrm{Res}(\langle W\rangle, T_{\mathrm{pol}}) \\
&= \frac{1}{16\pi}\int dx_0 \sum_{T_{\mathrm{pol}}} \frac{1}{T_{\mathrm{pol}}^3} e^{-m^2 T_{\mathrm{pol}}}\mathrm{Res}(\langle W\rangle, T_{\mathrm{pol}}). \qquad (3.14)
\end{aligned}$$

Here the sum goes over all pole positions T_{pol}. For the constant E field this reads

$$\begin{aligned}
\mathrm{Im}\Gamma^1 &= \frac{1}{16\pi}\int dx_0 \sum_{k=1}^{\infty}\left(\frac{eE}{k\pi}\right)^3 e^{-m^2\frac{k\pi}{eE}}\mathrm{Res}\left(\frac{TeE}{\sin(TeE)}, T = \frac{k\pi}{eE}\right) \\
&= \frac{V}{16\pi}\sum_{k=1}^{\infty}(-1)^k\left(\frac{eE}{k\pi}\right)^2 e^{-m^2\frac{k\pi}{eE}}, \qquad (3.15)
\end{aligned}$$

where V denotes the space-time volume. Since the first order of the effective action, the classical action, is real, this is the complete imaginary part of the effective action up to one-loop order. It is very remarkable that the result (3.15) has an essential singularity in the limit $e \to 0$. This shows explicitly, that pair creation is a nonperturbative effect which cannot be calculated by

a series expansion in the coupling constant. Thus it is essential to consider *all* one-loop diagrams.

For weak fields, the exponential term suppresses terms with large k and the sum is dominated by the first term:

$$\mathrm{Im}\Gamma \approx -\frac{V}{16\pi^3}(eE)^2 e^{-m^2\frac{\pi}{eE}}. \tag{3.16}$$

In the strong field limit, the exponential term is approximately 1 for the dominating terms and we obtain

$$\mathrm{Im}\Gamma \approx \frac{V}{16\pi}\left(\frac{eE}{\pi}\right)^2 \sum_{k=1}^{\infty}\frac{(-1)^k}{k^2} = -\frac{V}{192\pi}(eE)^2 \tag{3.17}$$

In the following, we will use these analytical findings to test the results of our numerical method during the process of development.

3.2.2 Numerical Computation: Straightforward Approach

In Minkowski space, a homogeneous electric field in x^1 direction is given by the potential $A_{\mathrm{M}} = (-Ex^1, 0, 0, 0)^\top$. The corresponding Euclidean potential reads $A = (0, 0, 0, -iEx_1)^\top$ and we have

$$F_{\mu\nu} = \begin{pmatrix} 0 & 0 & 0 & 0 \\ 0 & 0 & 0 & -iE \\ 0 & 0 & 0 & 0 \\ 0 & iE & 0 & 0 \end{pmatrix}. \tag{3.18}$$

Note that E always denotes the physical Minkowski-valued field strength. Owing to parity invariance, we only need the even part of the Wilson loop

$$\begin{aligned} W_{\mathrm{e}} &= \cos\left(e\int_0^1 dt\ \sqrt{T}\dot{y}_4\left(-iE\left(\sqrt{T}y_1 + x_{01}\right)\right)\right) \\ &= \cos(iTeEI), \end{aligned} \tag{3.19}$$

where $I := \int_0^1 dt\ \dot{y}_4 y_1$. We insert W_{e} into the renormalized one-loop effective action (2.49) and obtain

$$\Gamma^1 = -\frac{1}{(4\pi)^2}\int_0^\infty \frac{dT}{T^3}e^{-m^2T}\int dx_0\left(\langle\cos(iTeEI)\rangle - 1 - \frac{1}{6}T^2e^2E^2\right). \tag{3.20}$$

Actually $W_\mathrm{e} = \cosh(TeEI)$ and the argument is real. That means, W_e is exponentially increasing in T for all paths. This agrees with the fact that the expectation value has poles on the T axis as we already know from the analytical calculations. The increase of W_e is canceled by the mass term only for paths with $I < \frac{m^2}{eE}$. As in the analytical evaluation, we therefore have to find an appropriate integration contour for the T integration in the complex plane, but things are more subtle for the numerical approach. In our numerical algorithm, we can only use *finite* loop ensembles. There will be one loop that maximizes I for a given ensemble. For a value of T with large real part $\mathrm{Re}T$, this single loop will dominate the expectation value. In this case, the numerics breaks down, since the finite loop ensemble is no longer representative for the infinite ensemble of the path integral. In fact, the numerics already breaks down for smaller $\mathrm{Re}T$. The dominance of one single loop is merely the extreme case of a more general overlap problem.

We cannot numerically compute the Wilson loop expectation value for *all* points of any path in the T-plane with $\mathrm{Re}T \to \infty$. As a way out, we rotate the T integration contour onto the positive imaginary axis to end up with an expression which has the structure of a Fourier transform. With $\xi := -iT$ it reads

$$\begin{aligned}\Gamma^1 &= \frac{1}{(4\pi)^2}\int_0^\infty \frac{d\xi}{\xi^3} e^{-im^2\xi} \int dx_0 \left(\langle \cos(\xi eEI)\rangle - 1 + \frac{1}{6}\xi^2 e^2 E^2 \right) \\ &\overset{s=\xi eE}{=} \left(\frac{eE}{4\pi}\right)^2 \int dx_0 \int_0^\infty ds\; e^{-i\frac{m^2}{eE}s} \left(\frac{\langle \cos(sI)\rangle - 1}{s^3} + \frac{1}{6s} \right). \qquad (3.21)\end{aligned}$$

Since this s integral has the form of a Fourier integral with frequency $\frac{m^2}{eE}$, we can know use the Fast Fourier Transform (FFT) to compute Γ^1 for a whole spectrum of $\frac{m^2}{eE}$ all at once. However, from the numerical viewpoint, new difficulties arise: The expectation value comes with the statistical error. As a consequence, fine structures of the T dependence cannot be resolved. We do not expect to obtain information about the high frequency spectrum, that means for large $\frac{m^2}{eE}$. Unfortunately this range is of importance because it includes the weak field limit. A second problem is the error propagation. The standard FFT routines cannot give an estimate of the spectrum's errors for given errors of the input data. Modifying the standard routines cannot solve this problem without increasing the runtime significantly.

We try to avoid the described difficulties by interchanging propertime and path integral, i.e., first performing the propertime integral and taking

the expectation value afterwards. Γ^1 now reads

$$\Gamma^1 = \left(\frac{eE}{4\pi}\right)^2 \int dx_0 \left(\left\langle \int_0^\infty ds\ e^{-i\frac{m^2}{eE}s} \frac{\cos(sI)-1}{s^3} \right\rangle + \int_0^\infty ds\ e^{-i\frac{m^2}{eE}s} \frac{1}{6s} \right).$$

The imaginary part of the effective action, which we are focusing on, becomes

$$\begin{aligned} \mathrm{Im}\Gamma &= -\left(\frac{eE}{4\pi}\right)^2 \int dx_0 \left(\left\langle \int_0^\infty ds\ \sin\left(\frac{m^2}{eE}s\right) \left(\frac{\cos(Is)-1}{s^3}\right) \right\rangle + \frac{\pi}{12} \right) \\ &= -\left(\frac{eE}{4\pi}\right)^2 \int dx_0 \left(\left\langle \int_0^\infty ds\ \sin\left(\frac{m^2}{eE}s\right) \frac{-2\sin^2\left(\frac{I}{2}s\right)}{s^3} \right\rangle + \frac{\pi}{12} \right) \\ &= -\left(\frac{eE}{4\pi}\right)^2 \int dx_0 \left(\langle F \rangle + \frac{\pi}{12} \right) \end{aligned} \tag{3.22}$$

where we have analytically performed the propertime integral and introduced (see Fig. 3.2).

$$F = \begin{cases} -\frac{\pi}{2}\frac{m^2}{eE}(|I| - \frac{1}{2}\frac{m^2}{eE}) & , \quad 0 \le \frac{m^2}{eE} \le |I| \\ -\frac{\pi}{4}I^2 & , \quad |I| < \frac{m^2}{eE} \end{cases} \tag{3.23}$$

Obviously the last step, the analytical Fourier transform to obtain F, is

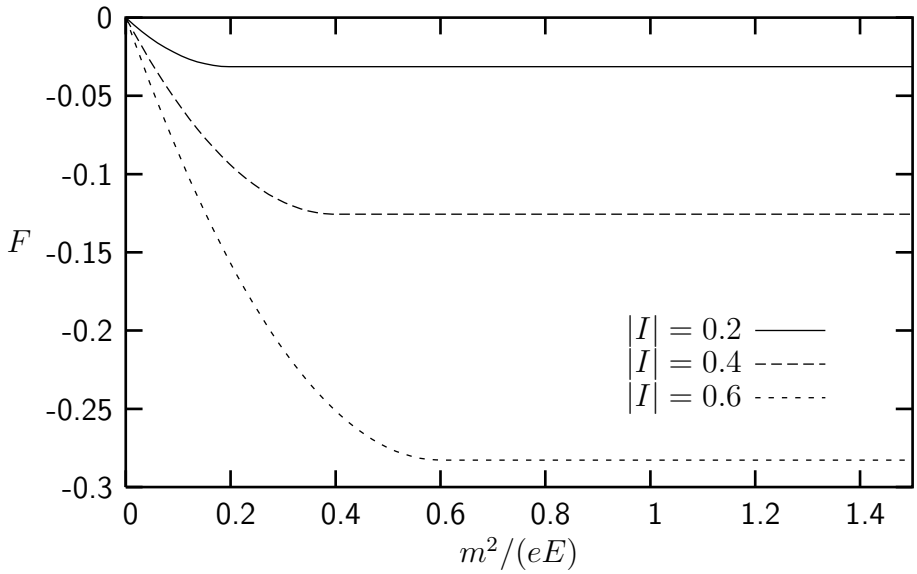

Figure 3.2: F for different values of $|I|$ as function of $\frac{m^2}{eE}$

only possible in the very special case of a constant E field. In more complex settings, we must bank on FFT.

In Fig. 3.3 the result of the numerical calculation is compared to the Schwinger effective action. For the FFT we have used the *sinft* routine combined with the *realft* algorithm, both from *Numerical Recipes* [46]. We have truncated the Fourier integral at $s = 128$ and used 8192 data values. The loop ensemble consisted of 5000 loops with 1000 ppl each.

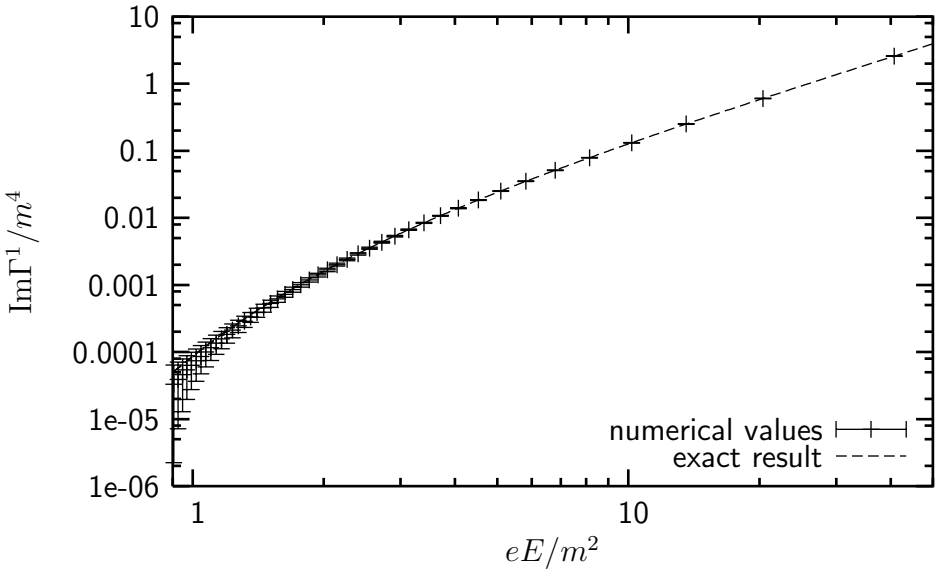

Figure 3.3: Imaginary part of the effective action for strong homogeneous electric fields. $n_{\mathrm{L}} = 5000$, $N = 1000$ ppl.

The described method works for small $\frac{m^2}{eE}$, i.e., strong fields. It yields exact results in the strong-field limit: The original function in Eq. (3.22) drops off with $\frac{1}{s^3}$. For sufficiently large frequency $\frac{m^2}{eE}$, the first sine increases very slowly with s, such that the overlap of the two factors vanishes in the limit $\frac{m^2}{eE} \to 0$ and the s integral gives zero for all I, even if performed numerically. Under these circumstances the expectation value $\langle F \rangle$ in Eq. (3.22) is zero, too, and Eq. (3.22) gives our analytical result (3.17).

However, the error bars become large for weak fields. It is the shape of the spectrum F, which is responsible for this.

The spectrum $F(\frac{m^2}{eE})$ has a non-compact support. However, discrete Fourier transform only works for bandwidth limited functions because the finite sample rate limits the maximal frequency resolved to the half of its own value. In our case, FFT provides the correct spectrum for lower frequencies, i.e. strong fields, it fails for high frequencies. However, by enhancing the

sample rate, that is evaluating the Wilson loop for more s values, we can extend the range of the calculations at the expense of CPU time.

Even if we could master the numerical Fourier transform or, in case of the constant field, use the analytical Fourier transform, we are restricted to strong fields. The reason for this is demonstrated in figure 3.2: For weak fields, the F values for different I are widely spread. As a result, the expectation value in this range comes with a large statistical error. In Eq. (3.22) the expectation value is shifted by $\frac{\pi}{12}$ and gets close to zero, whereas the statistical error stays untouched. Thus the shift leads to huge relative errors. Of course, for constant E we can find an expression for the distribution of I in the loop ensemble analytically, cf. section 3.3.3, and compute the exact expectation value of F, but again we want to make use of worldline numerics with more general field configurations in mind.

We put on record that we have found a useful routine for field strengths E roughly larger than the critical field strength $\frac{m^2}{e}$. In the next section we will search a workaround for the treatment of weaker fields.

3.2.3 Treatment of Weaker Fields

Both difficulties of the last section, the failing of the discrete Fourier transform and the large statistical error for weak fields, are rooted in the infinite support of the spectrum F. In turn, the infinite support of F is enrooted in the quadratic order of the original function in (3.22):

$$\frac{-2\sin^2\left(\frac{I}{2}s\right)}{s^3} = \frac{1}{s^3}\left(-\frac{I^2}{2}s^2 + \mathcal{O}(s^4)\right) = -\frac{I^2}{2s} + \mathcal{O}(s). \tag{3.24}$$

The Fourier transform of $-\frac{I^2}{2s}$ is $-\frac{\pi}{4}I^2 = \lim_{E\to 0} F$. It is precisely this term, which is responsible for the unlimited spectrum. The expectation value of its Fourier transform is

$$\langle -\frac{\pi}{4}I^2\rangle = \langle \lim_{E\to 0} F\rangle = \lim_{E\to 0}\langle F\rangle = -\frac{\pi}{12} \tag{3.25}$$

The last equality holds because $\lim_{E\to 0}\mathrm{Im}\Gamma = 0$ and thus $\lim_{E\to 0}\langle F\rangle$ has to cancel the $+\frac{\pi}{12}$ in Eq. (3.22).

The $+\frac{\pi}{12}$ comes from $\frac{1}{12}(TeF_{\mu\nu})^2$ in (2.49) which corresponds to the renormalization counterterm to compensate for the quadratic order of $\langle W\rangle$. Instead of compensating the quadratic order of the Wilson loop expectation value as a whole, we can cancel the quadratic order W_2 of each Wilson loop

separately. This conforms to using $\langle W_2 \rangle = -\frac{1}{12}(TeF_{\mu\nu})^2$ in (2.49) which leads to

$$\Gamma^1 = -\frac{1}{(4\pi)^2}\int_0^\infty \frac{dT}{T^3} e^{-m^2 T} \int dx_0 \left(\langle W - W_2 \rangle - 1\right). \tag{3.26}$$

In place of (3.22) we obtain

$$\begin{aligned} \mathrm{Im}\Gamma^1 &= -\left(\frac{eE}{4\pi}\right)^2 \int dx_0 \left\langle \int_0^\infty ds \ \sin\left(\frac{m^2}{eE}s\right) \left(\frac{-2\sin^2\left(\frac{I}{2}s\right)}{s^3} + \frac{I^2}{2s}\right) \right\rangle \\ &= -\left(\frac{eE}{4\pi}\right)^2 \int dx_0 \, \langle F_R \rangle \end{aligned} \tag{3.27}$$

with

$$F_R = \begin{cases} -\frac{\pi}{2}\frac{m^2}{eE}(|I| - \frac{1}{2}\frac{m^2}{eE}) + \frac{\pi}{4}I^2 & , \quad 0 \le \frac{m^2}{eE} \le |I| \\ 0 & , \quad |I| < \frac{m^2}{eE} \end{cases} \tag{3.28}$$

(see Fig. 3.4). F_R has a compact support, in contrast to F. In general, if the

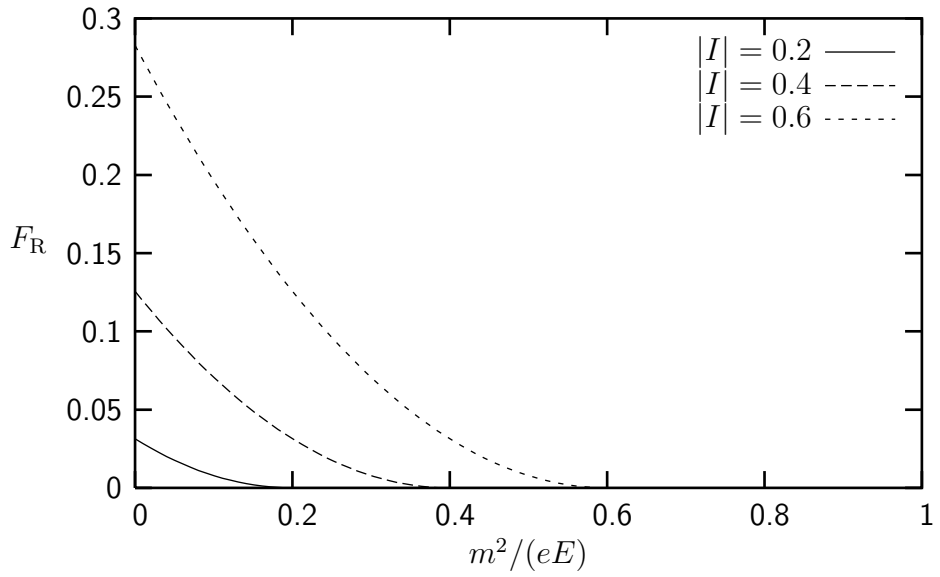

Figure 3.4: F_R for different values of $|I|$

third coefficient W_2 is not known analytically, it can be obtained by fitting a polynomial to W for small T. We know the first two Taylor coefficients to be 1 and 0, due to the fact that the argument of the cosine in (2.36) vanishes for $T = 0$ (in the constant-field case even all odd orders are zero). In practice

the fit to obtain the higher orders corresponds to solving

$$\begin{pmatrix} \triangle T^2 & \cdots & \triangle T^n \\ \vdots & \ddots & \vdots \\ ((n-1)\triangle T)^2 & \cdots & ((n-1)\triangle T)^n \end{pmatrix} \begin{pmatrix} W_2 \\ \vdots \\ W_n \end{pmatrix} = \begin{pmatrix} W(\triangle T) - 1 \\ \vdots \\ W((n-1)\triangle T) - 1 \end{pmatrix}$$

using the inverted matrix, which gives the coefficients a_i of a fitted polynomial of nth order. This procedure is faster than $lfit$, which is important as it needs to be performed several thousand times more often than the fit in the previous section.

Using (3.27) not only makes it possible to obtain the Fourier transform for the whole spectrum by FFT, but also shifts the range of large statistical error from large $\frac{m^2}{eE}$ to strong fields. Both leads to better results for field strengths below $\frac{eE}{m^2} \approx 2.2$, as demonstrated in Fig. 3.5. For this figure we already used the polynomial fit to obtain W_2, with $n = 9$ and $\triangle TeE = 1/8$, i.e. we fitted between $TeE = 0$ and $TeE = 1$. The statistical error is even small for stronger fields, but the strong-field limit is not reproduced exactly as in the previous method, due to the dependence of F_R on I for $\frac{m^2}{eE} = 0$ (see Fig. 3.4).

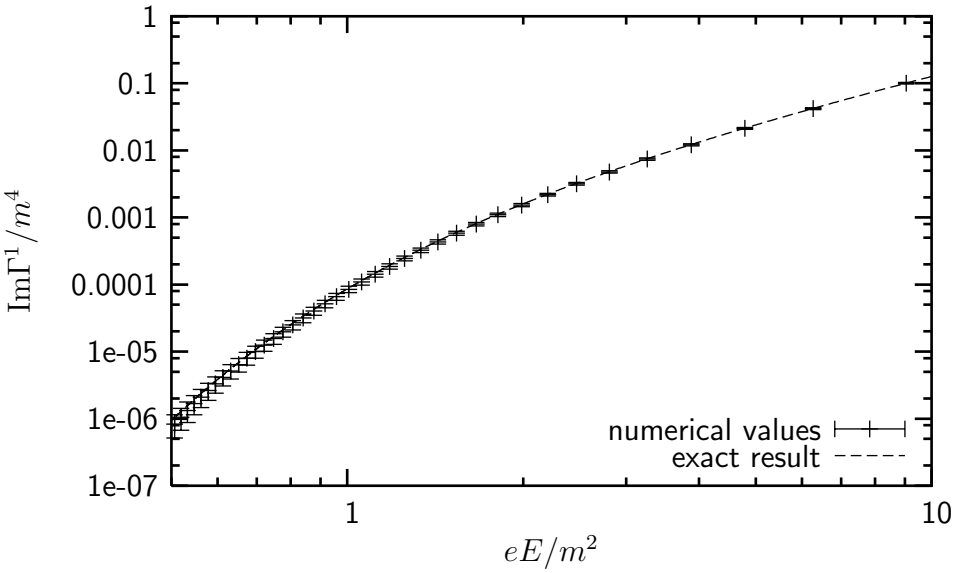

Figure 3.5: Imaginary part of the effective action for weaker homogeneous electric fields. $n_\mathrm{L} = 5000$, $N = 1000$ ppl.

However, for weak fields from $\frac{eE}{m^2} \approx 0.4$ downwards, the numerical results are not convincing. Figure 3.5 foreshadows a drop of the numerical values for

$\frac{eE}{m^2} < 0.4$. In fact our approach underlies principal limitations. For each loop with certain value I, F_R is zero for $\frac{m^2}{eE} > |I|$ (see Eq. (3.28) and Fig. 3.4). This implies that every loop contributes information about the dependence of the effective action's imaginary part on the field strength only for $\frac{m^2}{eE} < |I|$. In other words: For loops with $|I| < \frac{m^2}{eE}$, the background field is simply not existent. Since we use *finite* loop ensembles, there is a value for $\frac{eE}{m^2}$ below which *no* loop at all gathers information about the background concerning the imaginary part. In this case the exponent of the Wilson loop $TeEI$ is

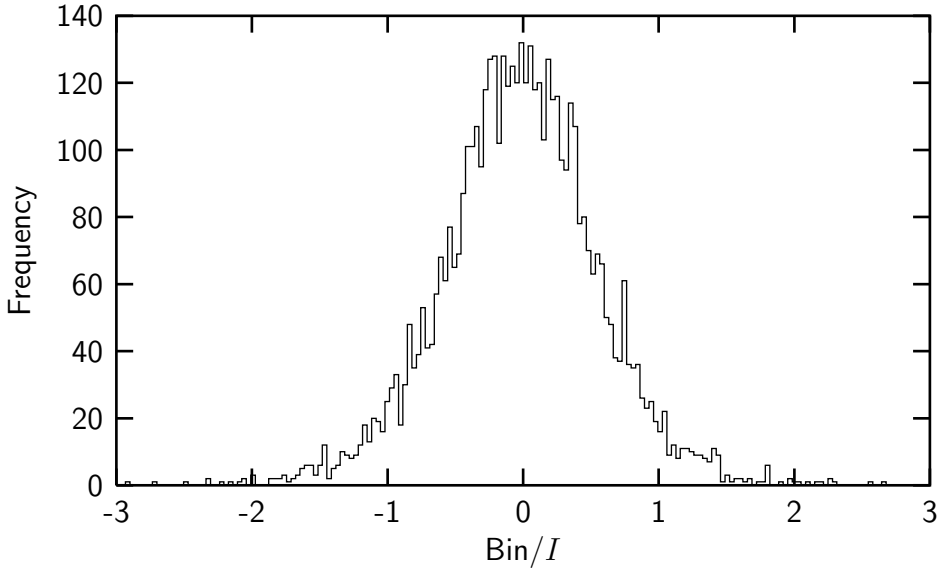

Figure 3.6: Typical distribution of $I = \int_0^1 dt\ \dot{y}_0 y_1$. $n_{\mathrm{L}} = 5000$, $N = 1000$.

smaller than m^2T for all loops. Consequently the T integral in Eq. (2.49) is finite for each single loop, no naive divergences occur and thus the integral has no imaginary part.

Figure 3.6 shows a typical distribution of I for an ensemble of 5000 loops. Only four loops have values $|I| > 2.5$, i.e. F_R is unequal zero at $\frac{eE}{m^2} = 0.4$. Consequently we expect the statistical error to fail in giving a proper estimate of the numerical accuracy for weak fields. In fact, in our example no loop gives $|I| > 3$. As a consequence the calculation yields $\mathrm{Im}\Gamma^1 = 0$ for $\frac{eE}{m^2} < \frac{1}{3}$ in contrast to the exact result, while the corresponding statistical error is zero (at least if the Fourier integral was performed analytically).

We will analytically calculate the distribution function of I in section 3.3.3, but we can already use the present result to gain a more concise idea

of the limitations. The distribution function reads

$$P(I) = \frac{\pi}{4} \frac{1}{\cosh^2(\frac{\pi}{2} I)}. \tag{3.29}$$

The proportion of loops with $|I|$ larger than a certain value I_0 is $2/(1+e^{\pi I_0})$. That means, for a given number of loops n_L, the value I_0, which is exceeded by $|I|$ for on average n loops, is

$$I_0 = \frac{1}{\pi} \ln \left(2\frac{n_L}{n} - 1 \right). \tag{3.30}$$

If n is the minimal number of loops that contribute information about the background to the effective action to obtain a reasonable result, we find that $E_{\min} = \frac{m^2}{eI_0}$ is a lower bound for the treatable field strength. Unfortunately Eq. (3.30) shows that I_0 goes merely logarithmically with n_{L}, which itself is proportional to CPU time. This inhibits to downsize $E_{\min}$ considerably by pure brute force.

Even though our approach so far was related to the constant-field case, we do not expect to find less limitations for more complex background fields. In general one can say, the loop cloud provided by the vloop algorithm does not deliver enough direct information about weak-field scenarios. One option is the modification of the distribution of paths in the loop ensemble, such that there are more loops with larger $|I|$, and subsequent reweighting of the Wilson loop values when calculating the expectation value. In the next subsection we present a different method which guarantees exact results in the weak field limit.

3.2.4 Weakest Fields: Pole Fit

In Eq. (3.14) we wrote the imaginary part of the effective action as sum over the residues of the Wilson loop expectation value. The weaker the fields the smaller the contribution of poles at large T, due to the damping mass term. In the weak-field limit only the first pole contributes. In other words, if the residues and positions of the first poles are known, the imaginary part of the effective action can be predicted very precisely for weak fields.

For field configurations obtained by steady deformation of the constant field, we expect the Wilson loop expectation value to emerge from the constant field's $\langle W \rangle$ by steady deformation, too. Our strategy is the following: Taking the exact Wilson loop expectation value for the constant field (3.13),

we introduce several parameters to obtain a more general function of T. This function is fitted to the numerical Wilson loop expectation values for non-constant fields, defining the values of the parameters. Afterwards, the poles of the fitted function are obtain analytically.

Of course it is important to make a reasonable choice for the introduced parameters. We make the assumption, that for any field configuration the poles of $\langle W \rangle$ only differ from the constant-field poles in their position on the real axis and the real part of the residuals. For each pole of (3.13) we will introduce two parameters, controlling these quantities.

We can write $TeE/\sin(TeE)$ as sum:

$$\begin{aligned}
\frac{TeE}{\sin(TeE)} &= 1 + \frac{(TeE)^2}{\pi} \sum_{\substack{k=-\infty \\ k\neq 0}}^{\infty} \frac{(-1)^k}{k(TeE - \pi k)} \\
&= 1 + \sum_{\substack{k=-\infty \\ k\neq 0}}^{\infty} (-1)^k \frac{eE}{\pi k} \frac{T^2}{T - \frac{\pi k}{eE}} \\
&= 1 + \sum_{\substack{k=-\infty \\ k\neq 0}}^{\infty} a_k \frac{T^2}{T - b_k}, \qquad (3.31)
\end{aligned}$$

with $a_k = (-1)^k \frac{eE}{\pi k} = \mathrm{Res}(TeE\ \mathrm{cosec}(TeE), T = b_k)/b_k^2$ and $b_k = \frac{\pi k}{eE}$.

We use a_k and b_k as the above mentioned parameters and vary them to fit Eq. (3.31) to the numerical Wilson loop expectation values.

Actually we do not fit (3.31), but a slightly simplified expression. $\langle W \rangle$ is always even in T, that means a_k and b_k are antisymmetric in k. Consequently we can write

$$\langle W \rangle = 1 + 2T^2 \sum_{k=1}^{\infty} \frac{a_k b_k}{T^2 - b_k^2}. \qquad (3.32)$$

Of course, in practice the infinite sum has to be approximated by a finite one, leaving us with a finite number of parameters.

Once the parameters are determined, the imaginary part of the effective action is calculated as in (3.14):

$$\begin{aligned}
\mathrm{Im}\Gamma^1 &= \frac{-1}{(4\pi)^2} \int dx_0\ \mathrm{Im} \sum_{k=1}^{\infty} \frac{1}{{b_k}^3} e^{-m^2 b_k} (-\pi i) \mathrm{Res}\left(\langle W \rangle, T = b_k\right) \\
&= \frac{1}{16\pi} \int dx_0 \sum_{k=1}^{\infty} e^{-m^2 b_k} \frac{a_k}{b_k}. \qquad (3.33)
\end{aligned}$$

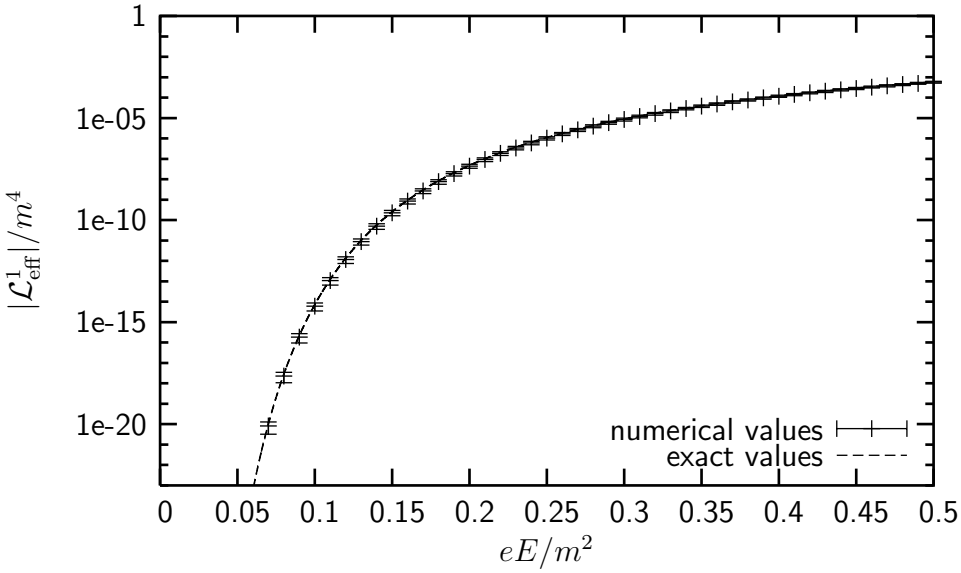

Figure 3.7: The imaginary part of the effective Lagrangian for the constant pure electric field: exact result in comparison with the numerical estimate obtained by pole fitting. $n_L = 5000$, $N = 1000$.

Figure 3.7 shows the absolute value of the effective Lagrangian obtained by the pole-fitting procedure, using the same loop ensemble as in the previous figures. For the same reason by which we rotated the T integration contour onto the imaginary axis in 3.2.2, the fit-function (3.32) has been fitted to $\langle W \rangle$ for imaginary T. We have used 15 values between 0 and $TeE = i/2$ and fitted ten parameters. That means we have truncated the progression in the fit-function (3.32) after five terms. If procurable one should use more terms, since in our fitting range the terms with $k > 5$ contribute up to 14% to the complete sum. Larger fitting ranges mean even larger contributions. Yet using more fitting parameters requires the use of more loops to reduce the statistical error.

Despite the fact that we have used only five terms of the progression, the values for the effective action are convincing. This arises from the fact that the effective action is dominated by the first pole which is determined very precisely by the fit. Apparently the terms of higher k compensate for the truncation of the progression. Their poles are not correctly determined, but they do not contribute to the effective action because of the damping mass

term in (3.33).

The pole fitting procedure has no lower limit for the field strength E. On the contrary, the weaker the field, the better it works, as the domination of the effective action by the first pole increases. Stronger fields can be accessed by considering more poles in the fit function, that is including terms of higher k.

3.2.5 Conclusion

We presented three algorithms to compute the effective action for the constant pure E field. Each has its own range of use: weak, medium and strong fields, respectively. Now that we have subdued the constant electric field with worldline numerics, we turn towards inhomogeneous field configurations.

3.3 The Sauter Potential

The Sauter Potential defines a spatial inhomogeneous but temporally constant electric field, for which an analytical expression of the corresponding total pair production is known. In Minkowskian space the potential reads

$$A^0_{\mathrm{M}} = -a\tanh(kx^1), \tag{3.34}$$
$$A^i_{\mathrm{M}} = 0, \quad i=1,2,3. \tag{3.35}$$

The x^1 component of the corresponding field is

$$E^1_{\mathrm{M}} = \frac{ak}{\cosh^2(kx^1)} \tag{3.36}$$

whereas the other components are zero (see Fig. 3.8). That means the field is equally oriented in the whole space, in our coordinates in x^1 direction which is also the only direction in which the strength varies. The field is strongest at $x^1=0$, where it amounts to $|E|=ak$, and drops off on both sides. The parameter k is a size parameter: its inverse k^{-1} determines the extent of the Sauter potential in x^1 direction.

The imaginary part of the corresponding effective action can be written as an integral expression [39]:

$$\mathrm{Im}\Gamma = \frac{V}{8\pi^2}\int_0^{\sqrt{(ea)^2-m^2}} dp_\perp p_\perp \int_{-ea+\sqrt{p_\perp^2+m^2}}^{ea-\sqrt{p_\perp^2+m^2}} dp^0 \ln\left(1-\frac{\sinh(2\pi\mu)\sinh(2\pi\mu)}{\sinh^2(\pi(\mu+\nu))+\cos^2(\pi\tilde{\lambda})}\right).$$

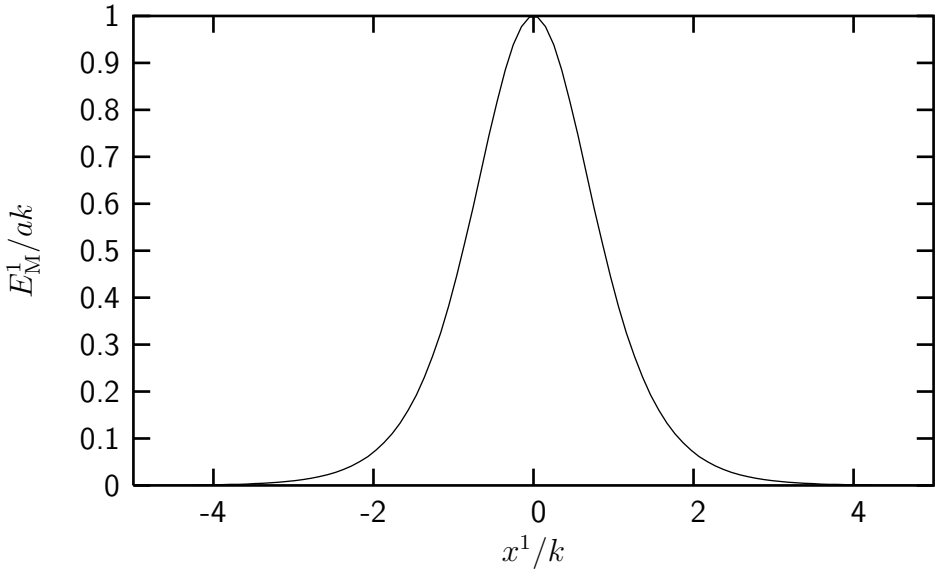

Figure 3.8: The electric field corresponding to the Sauter potential.

Here, V denotes the space-time volume and we have used the following abbreviations:

$$\mu, \nu := \frac{1}{2k}\sqrt{(p^0 \pm ea)^2 - p_\perp^2 - m^2}, \tag{3.37}$$

$$\tilde{\lambda} := \sqrt{\frac{1}{4} - \left(\frac{ea}{k}\right)^2}. \tag{3.38}$$

For given parameters a and k, the integrals can be performed numerically, e.g., by use of *Mathematica*. One qualitative property is apparent: the integration intervals vanish if $|ea| = m$. This reflects the fact that pairs are produced only if particle and anti-particle are separated by a difference in potential energy that is larger than the total mass of the pair. For the Sauter potential, the potential energy differs between $x^1 = -\infty$ and $x^1 = +\infty$ by $2ea$, which has to be compared to the mass of two particles $2m$. This leads to the condition $|ea| > m$. Otherwise ImΓ is zero.

3.3.1 Worldline Numerics: Preceding Advisement

In Euclidean space, the Sauter potential reads

$$A_4 = -ia\tanh(kx_1), \tag{3.39}$$

$$A_i = 0, \quad i = 1, 2, 3. \tag{3.40}$$

Inserting the Sauter potential into the even part of the Wilson loop (2.36) yields

$$\begin{aligned} W_\mathrm{e} &= \cos\left(e\int_0^1 dt\ \sqrt{T}\dot{y}_4(-i)a\tanh\left(k\left(\sqrt{T}y_1+x_0\right)\right)\right) \\ &= \cosh\left(\sqrt{T}ea\int_0^1 dt\ \dot{y}_4\tanh\left(k\left(\sqrt{T}y_1+x_0\right)\right)\right). \end{aligned} \tag{3.41}$$

In general, we have

$$\tanh(x)\to\begin{cases} 1, & \text{for } \mathrm{Re}x\to\infty \\ -1, & \text{for } \mathrm{Re}x\to-\infty \end{cases}. \tag{3.42}$$

Thus, in the limit $\mathrm{Re}\sqrt{T}\to\pm\infty$, the hyperbolic tangent in Eq. (3.41) becomes a sign function. Speaking in terms of loop clouds: if the loop cloud is expanded by a large factor $\mathrm{Re}\sqrt{T}$, it does not realize the small-scale information about the hyperbolic tangent in the range of the origin, but only the large-scale information, which is the same as for the sign function $\sigma(k\sqrt{T}y_1)$. For the even part of the Wilson loop this means

$$W_\mathrm{e}\overset{|\mathrm{Re}\sqrt{T}|\gg1}{\approx}\cosh\left(\sqrt{T}ea\int_0^1 dt\ \dot{y}_4\sigma(y_1)\right). \tag{3.43}$$

Similarly to the constant field case discussed in section 3.2.2, W_e diverges for $|\mathrm{Re}\sqrt{T}|\to\infty$. If $|\mathrm{Re}\sqrt{T}|$ becomes large, the expectation value $\langle W\rangle=\langle W_\mathrm{e}\rangle$ will be dominated by the loop which maximizes $\int_0^1 dt\ \dot{y}_4\sigma(y_1)$. The only way to circumvent this, is to prevent $|\mathrm{Re}\sqrt{T}|$ from becoming large by choosing an integration contour close to the negative real axis. Though with that choice, the t integration of a given loop will hit the poles of the hyperbolic tangent, if $|T|$ goes to infinity. Thus we have to conclude, that we cannot compute the Wilson loop expectation value for arbitrary large $|T|$ with worldline numerics.

The straight forward approach to compute the effective action, evaluating the Wilson loop expectation value and integrating over T afterwards, is not feasible for the Sauter potential, as, for all possible integration contours, $|T|$ goes to infinity. Thereby, two of the three methods we have developed for the constant pure electric field find no analogue for the Sauter potential: both, the strong field algorithm, presented in section 3.2.2, and its variation for weaker fields, section 3.2.3, use an explicit contour integration in the complex T plane. In the following we will study the adaptability of the pole fitting procedure. From the experimental view, this is the most interesting one, since experimental realizations are far from reaching field strengths that can be treated by the other methods.

3.3.2 Pole Fit

The considerations of the preceding section taught us, that worldline numerics provides the Wilson-loop expectation value only for T values from a relatively small environment of $T = 0$. Thus the pole fit is restricted to a small interval. Facing the numerous fitting parameters we used in 3.2.4, very small statistical errors of the Wilson loop expectation values are required. Some test runs show, that the fit is hardly feasible for loop clouds realizable on common computers. Accordingly, we have to rethink the fit function (3.32). It is rather discontenting that ten or more parameters are used but only two of them are required for our final result, the imaginary part of the effective action for weak fields. Starting from the analytical Wilson-loop expectation value for constant E, we try to introduce only two parameters:

$$\frac{TeE}{\sin(TeE)} \to a\frac{bT}{\sin(bT)}. \tag{3.44}$$

The parameters a and b control position and residue of all poles simultaneously, in particular of the first pole. But for small T, the fit function has to agree with the heat-kernel expansion, Eq. (2.40),

$$a\frac{bT}{\sin(bT)} = a + \frac{ab^2}{6}T^2 + \cdots \stackrel{!}{=} 1 + \frac{1}{6}(TeE(x_0))^2 + \cdots, \tag{3.45}$$

and as a consequence there is no freedom for adjusting the parameters. We extend the fit function in 3.44 by adding a third parameter to obtain $a\frac{bT}{\sin(bT)} + c$. With the knowledge of the heat-kernel expansion, two of the parameters can be expressed by the third one, leaving us with only one parameter,

$$\frac{T(eE)^2}{b\sin(bT)} + 1 - \frac{(eE)^2}{b^2}. \tag{3.46}$$

Admittedly, *one* fitting parameter is not sufficient to obtain *two* characteristics of $\langle W \rangle$, the residue and the position of the first pole. We have searched for further extensions of expression (3.46) involving more parameters, but have not found an obvious candidate for a *manifest* fit function. The reason lies in the existence of multi-local constraints: the pole structure of $\langle W \rangle$ and the small-T behavior have to be taken into account. Instead we will fit a function to a more fundamental quantity than the Wilson-loop expectation value, as described in the following.

3.3.3 CDF Fit

This subsection describes the development of our most efficient and most flexible algorithm that we recommend for general use. In the numerical computation of the Wilson-loop expectation value $\langle W\rangle$, the t integration in Eq. (2.39) reduces the information of each unit loop $y(t)$ to a single scalar quantity. In section 3.2.2, where the constant E field is treated, we have introduced $I = \int_0^1 dt\ \dot{y}_4 y_1$. Let us analytically compute the probability density function (PDF) $P(I)$. We have

$$\begin{aligned} P(I) &= \langle \delta(I - \int_0^1 dt\ \dot{y}_4 y_1)\rangle \\ &= \frac{1}{\mathcal{N}} \int \mathcal{D}y\ \delta(I - \int_0^1 dt\ \dot{y}_4 y_1)\ e^{-\int_0^1 dt\ \frac{\dot{y}^2}{4}}. \end{aligned} \tag{3.47}$$

Using the Fourier representation of the δ function, one obtains

$$P(I) = \int \frac{d\omega}{2\pi}\ e^{i\omega I} \frac{1}{\mathcal{N}} \int \mathcal{D}y\ e^{-i\omega \int_0^1 dt\ \dot{y}_4 y_1} e^{-\int_0^1 dt\ \frac{\dot{y}^2}{4}}. \tag{3.48}$$

The path integral is exactly the worldline representation of the Wilson-loop expectation value for a pure constant B field with $TeB = \omega$. We can revert to our previous result, Eq. (2.74):

$$\begin{aligned} P(I) &= \int \frac{d\omega}{2\pi}\ e^{i\omega I} \frac{\omega}{\sinh \omega} \\ &= \frac{\pi}{4} \frac{1}{\cosh^2 \frac{\pi}{2} I}. \end{aligned} \tag{3.49}$$

This expression is already normalized. The Wilson-loop expectation value in terms of $P(I)$ reads

$$\langle W\rangle = \int_{-\infty}^{\infty} dI\ P(I) W(I) \tag{3.50}$$

$$= \int_{-\infty}^{\infty} dI\ \frac{\pi}{4} \frac{1}{\cosh^2 \frac{\pi}{2} I} \cosh(TeEI) \tag{3.51}$$

$$= \frac{TeE}{\sin TeE}, \tag{3.52}$$

as it should, cf. Eq. (3.13).

For a non-constant field, we generalize the quantity I:

$$I := \frac{i \int_0^1 dt\ \dot{y} A(\sqrt{T} y + x_0)}{\sqrt{T} E_0}. \tag{3.53}$$

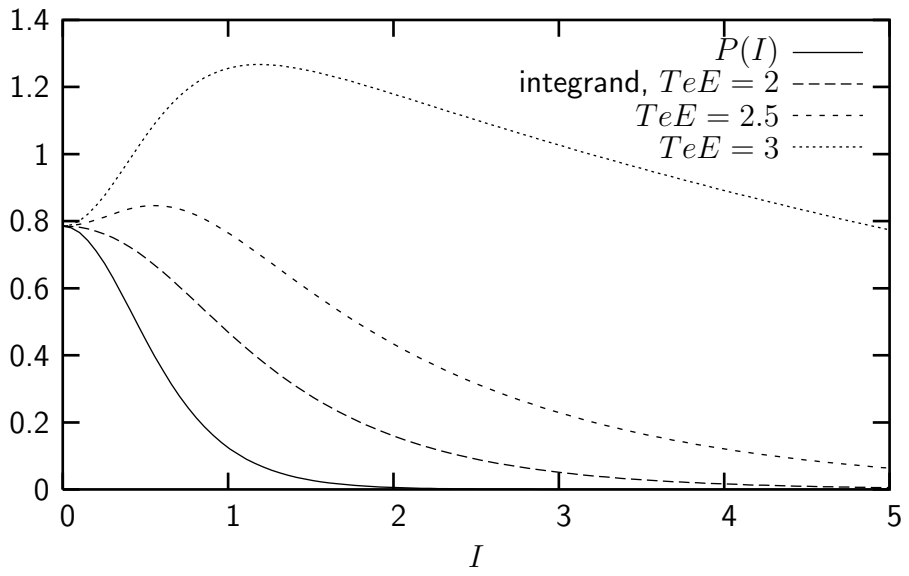

Figure 3.9: The probability distribution of I for the constant field and the integrand of the I integration in Eq. (3.51). For large TeE, the integrand contributes to the integral mainly for I values with very small $P(I)$.

The field strength E_0 in the denominator is a priori arbitrary and has been introduced to obtain a dimensionless quantity. In most cases we can use $E_0 := |E(x_0)|$. For the constant E field, our generalized definition of I conforms to the previous one. The Wilson-loop expectation value can be computed as in Eq. (3.50) for any field configuration, if the probability density function $P(I)$ is known:

$$\langle W \rangle = \int_{-\infty}^{\infty} dI \; P(I)W(I) = \int_{-\infty}^{\infty} dI \; P(I) \cosh(TeE_0 I). \tag{3.54}$$

The difficulty is that we face an overlap problem which we already encountered in section 3.2.2 and 3.3.1. There, it prevented us from computing the Wilson-loop expectation value for large ReT and Re$\sqrt{T}$, respectively. In Eq. (3.54), the probability density $P(I)$ will always be concentrated around $I = 0$ as in expression (3.49) in the constant-field case. However, if TeE_0 becomes large, the maximum of the complete integrand moves to values of I far from zero. Thus the relative overlap of $P(I)$ and the integrand decreases for increasing TeE_0. This is demonstrated in Fig. 3.9 for the constant field, where $P(I)$ and the integrand for different values of TeE are plotted. This is of importance since we use *finite* loop ensembles: with a shrinking overlap

the integral is dominated by a decreasing number of loops. We solve this problem by interpolating the numerically obtained probability distribution by a functional form that also extrapolates implicitly to I values larger than the largest value of the loop ensemble. In order to make contact with the numerical data, we make use of a fitting procedure. As for the pole fit we take the analytic result for the constant electric field, in this case $P(I) = \frac{\pi}{4}\frac{1}{\cosh^2 \frac{\pi}{2} I}$, and generalize it by introducing free parameters:

$$P_{\text{fit}}(I) = N \frac{1}{\cosh^{2\nu} \frac{\pi}{2} a I}. \tag{3.55}$$

The two positive parameters a and ν control the two main features of the probability density function $P_{\text{fit}}(I)$, the width and the sheerness, respectively. The normalization constant N is a function of a and ν. The constraint $\int_{-\infty}^{\infty} dI \; P_{\text{fit}}(I) = 1$ gives

$$N = \left(\int_{-\infty}^{\infty} dI \frac{1}{\cosh^{2\nu} \frac{\pi}{2} a I} \right)^{-1} = \frac{\sqrt{\pi} a \Gamma(\nu + \frac{1}{2})}{2\Gamma(\nu)}, \tag{3.56}$$

where Γ denotes the Euler gamma function.

In contrast to prior approaches, we are able to perform the I integral analytically, if a and ν are determined. This is advantageous as the integral in Eq. (3.54) is only well defined for TeE_0 smaller than a certain value. The exponentially increasing cosine hyperbolicus has to be damped by the probability distribution P. In the constant-field case, for example, this requires $TeE < \pi$, otherwise the integral (3.51) is divergent. Nevertheless, the result for small TeE has a well-defined analytic continuation into the whole complex plane: expression (3.52) holds for all values of TeE, except for the pole positions. In the pole-fit algorithm of section 3.2.4, we have computed the I integral numerically for small TeE, and have tried to find a continuation afterwards by fitting an analytic function to the computed values. Now, with the analytic integration, the continuation of the analytic result is immediate.

To obtain $\langle W \rangle$ for a given T, we apply the following procedure: I is computed for every loop of our ensemble. The fraction of loops with $|I|$ smaller than a given value $|I_0|$ provides us with an estimate for the cumulative density function (CDF), defined by

$$D(|I_0|) = \int_{-|I_0|}^{|I_0|} dI \; P(I) = 2 \int_0^{|I_0|} dI \; P(I). \tag{3.57}$$

We compute the estimate of $D(|I_0|)$ for several values of $|I_0|$ and fit them with the CDF corresponding to the PDF in Eq. (3.55),

$$D_{\text{fit}}(|I_0|) = 2\int_0^{|I_0|} dI\ P_{\text{fit}}(I) = 2\int_0^{|I_0|} dI\ N\frac{1}{\cosh^{2\nu}\frac{\pi}{2}aI}, \tag{3.58}$$

to determine the parameters a and ν. Figure 3.10 shows an example of a

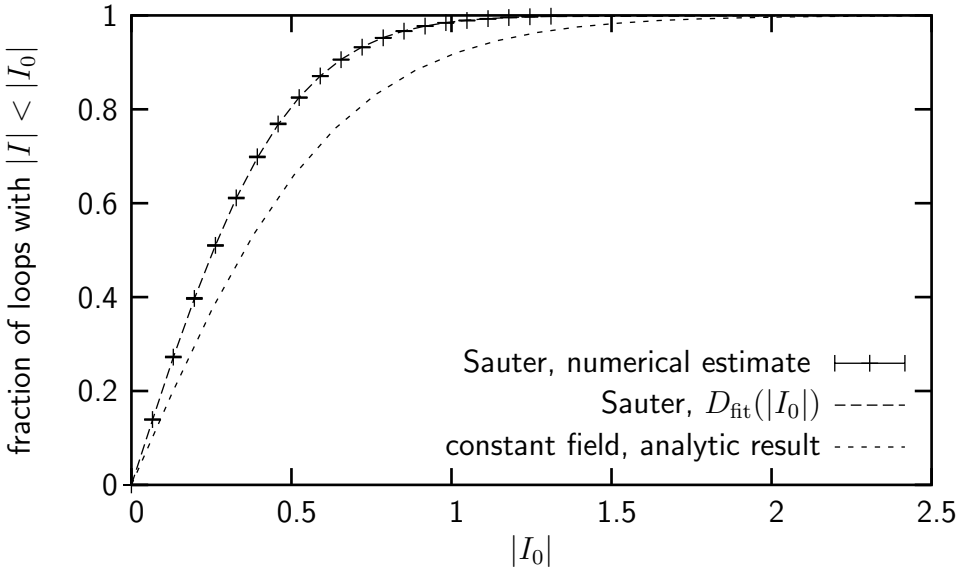

Figure 3.10: Example of a fitted cumulative density function (CDF) $D_{\text{fit}}(|I_0|)$ at $T = 10$ in the centre of a Sauter potential, compared to the numerical estimate. The exact CDF for the constant field is also shown for comparison. Parameters of the Sauter potential: $ea = \frac{3}{2}m$, $k = \frac{2}{3}m$. Parameters of the loop cloud: $n_{\text{L}} = 100000$, $N = 1000$ppl.

fitted CDF for the Sauter potential compared to the numerical estimate. Even though our ansatz (3.55) is very simple, the agreement is satisfactory. The figure also shows the exact CDF for the constant field,

$$D(|I_0|) = 2\int_0^{|I_0|} dI\ \frac{\pi}{4}\frac{1}{\cosh^2\frac{\pi}{2}I} = \tanh(\frac{\pi}{2}|I_0|). \tag{3.59}$$

In a final step, the probability density function P_{fit} with the parameters provided by the fit is inserted into Eq. (3.54) and the I integration is performed

analytically,

$$\begin{aligned}\langle W\rangle &= \int_{-\infty}^{\infty} dI\ N\frac{1}{\cosh^{2\nu}\frac{\pi}{2}aI}\cos(iTeE_0I)\\ &= N\frac{4^\nu}{\pi a}\frac{\Gamma(\nu+\frac{TeE_0}{\pi a})\Gamma(\nu-\frac{TeE_0}{\pi a})}{\Gamma(2\nu)}.\end{aligned} \tag{3.60}$$

The appearance of the gamma function, which has poles on the real axis, gives rise to the pole structure of the Wilson loop-expectation value. The latter is studied in more detail in the next section.

3.3.4 Application of the CDF Fit

Pole Positions

To compute the imaginary part of the effective action, we first have to determine the pole positions of the Wilson-loop expectation value Eq. (3.60), at least the position of the first pole on the real T axis.

The gamma function $\Gamma(x)$ has simple poles on the real negative axis at $x = 0, -1, -2, \cdots$. For positive T, the second gamma function in the numerator of (3.60) is responsible for the pole structure of $\langle W\rangle$. Poles occur, if

$$\nu - \frac{TeE_0}{\pi a} = -l \tag{3.61}$$

with $l = 0, 1, 2, \cdots$.

It should be stressed, that Eq. (3.60) does not reflect the full T dependence of $\langle W\rangle$. The I values have to be computed for a certain T value. The probability density function $P(I)$ depends on this value and so do the parameters a and ν which appear in Eq. (3.60) and Eq. (3.61). Hence the poles have to be searched for, repeating the CDF-fit procedure for different values of T.

An adequate, though optimizable, search routine is given by the following: As a first guess, we choose for the T value the pole position T_{p1} of $\langle W\rangle$ for a constant E field with field strength E_0 corresponding to, for instance, the local field strength of a given point x. The fitted parameters a and ν are then used in Eq. (3.61) to obtain a better estimate for the pole's T value,

$$T_{\mathrm{p2}} = \frac{\pi a(T_{\mathrm{p1}})}{eE_0}(\nu(T_{\mathrm{p1}}) + l). \tag{3.62}$$

When searching for the first pole, we use $l = 0$, additional poles are obtained by using higher l values. This step is repeated iteratively, until convergence is reached,

$$T_{\mathrm{p}i+1} = \frac{\pi a(T_{\mathrm{p}i})}{eE_0}(\nu(T_{\mathrm{p}i}) + l). \tag{3.63}$$

The iteration provides us with an estimate of the pole position T_{pol}, but is not well suited for error propagation. A simple method for still obtaining a reliable estimate for the statistical error of the pole position and moreover for any other secondary quantity of $\langle W \rangle$ is the *jackknife* analysis, that is reviewed in appendix A.2.

Once the position T of the first pole is determined, it gives a first information about the corresponding imaginary part of the effective action. The larger the T value, the more the contribution of the pole's residue to the effective action is suppressed by the factor e^{-m^2T}, cf. Eq. (3.14). We expect large T values, if small imaginary parts of the effective action are anticipated and vice versa.

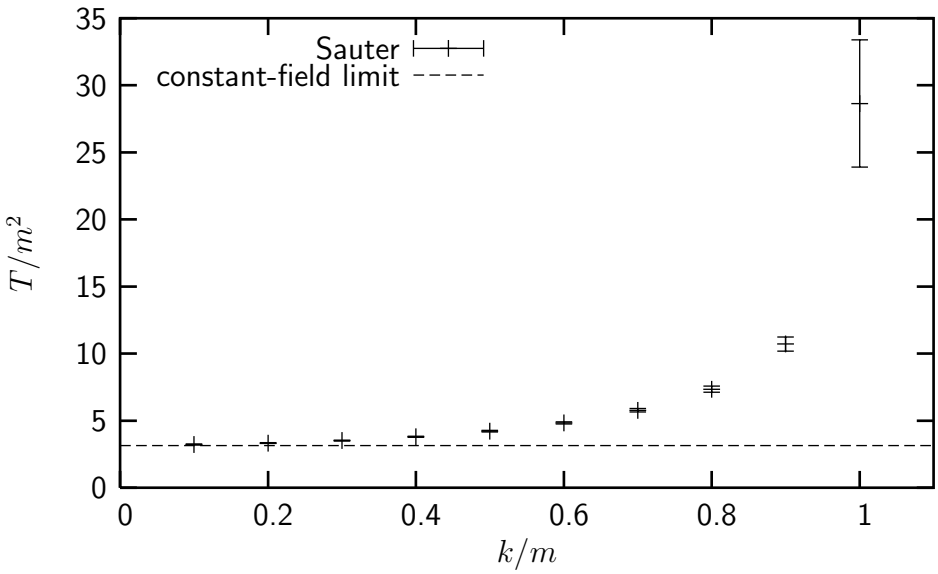

Figure 3.11: Position of the first pole of $\langle W \rangle$ in the centre of a Sauter potential with maximum field strength $\frac{m^2}{e}$ versus the width parameter k. The dashed line marks the analytic result for the constant-field limit $E \equiv \frac{m^2}{e}$ at $T/m^2 = \pi$. Parameters of the loop cloud: $n_{\mathrm{L}} = 100000$, $N = 1000$ppl.

For the Sauter potential we know the imaginary part of the effective

action to vanish if ea becomes equal to m. Consider a Sauter potential with the maximal field strength $E_{\max} = ak \equiv \frac{m^2}{e}$. We start with the limit $k \to 0$, i.e., a constant field of strength $E_{\max}$ with the first pole at $T/m^2 = \pi$. When increasing the parameter k, while keeping $E_{\max}$ fixed, the width of the field distribution decreases. Consequently we expect the pair production rate to decrease, whereas the T value of the pole position should increase. When k reaches $k = m$, which implies $ea = m$ and a vanishing pair production, the T value should approach infinity, such that no poles of the Wilson-loop expectation value should be detectable. Figure 3.11 shows the result of the CDF-fit procedure for the position of the first pole of $\langle W \rangle$ in the centre $x_1 = 0$ of the described Sauter potential versus the width parameter k. As expected, we recover the constant field result in the limit $k \to 0$ and the T value of the pole position increases with an increasing k. For $k = m$, we have expected it to go to infinity. Although we still find a pole in that case, the corresponding T value as well as its error estimate is very large. For $T/m^2 = 30$, the damping mass term $e^{-m^2 T}$ has the order of magnitude 10^{-15} which can be regarded as the numerical inaccuracy of a zero result.

This is an important and successful test of our CDF-fit procedure. Since the choice (3.55) for the fit function represents a potentially biassed assumption for the exact distribution, we have introduced a systematic error in our algorithm. This error cannot be controlled a priori, since the exact form of $P(I)$ and its important features cannot be predicted for an arbitrary inhomogeneous field. But, as this test case for the Sauter potential demonstrates surprisingly accurately, the systematic error of our procedure is vanishingly small even in an extremal case. We consider this as a strong evidence for the reliability of our procedure.

Residues

In order to determine the imaginary part of the effective action using Eq. (3.14), in addition to the positions of the poles of the Wilson-loop expectation-value, we need to determine their residues. We have

$$\begin{aligned} \operatorname{Res}\left(\Gamma\left(\nu - \frac{TeE_0}{\pi a}\right), T_{\text{pol}}\right) &= \frac{\operatorname{Res}(\Gamma, -l)}{\frac{d}{dT}\left(\nu - \frac{TeE_0}{\pi a}\right)\Big|_{T_{\text{pol}}}} \\ &= \frac{(-1)^l}{l!\,\frac{d}{dT}\left(\nu - \frac{TeE_0}{\pi a}\right)\Big|_{T_{\text{pol}}}}. \end{aligned} \tag{3.64}$$

Thus Eq. (3.60) yields

$$\mathrm{Res}(\langle W\rangle, T_{\mathrm{pol}}) = N\frac{4^\nu}{\pi a}\frac{\Gamma(\nu+\frac{T_{\mathrm{pol}}eE_0}{\pi a})}{\Gamma(2\nu)}\frac{(-1)^l}{l!\,\frac{d}{dT}\left(\nu-\frac{TeE_0}{\pi a}\right)\big|_{T_{\mathrm{pol}}}}. \tag{3.65}$$

For the first pole, i.e., $l=0$ and $\nu=\frac{TeE_0}{\pi a}$, this equation reads

$$\mathrm{Res}(\langle W\rangle, T_{\mathrm{pol}}) = N\frac{4^\nu}{\pi a}\frac{1}{\frac{d}{dT}\left(\nu-\frac{TeE_0}{\pi a}\right)\big|_{T_{\mathrm{pol}}}}. \tag{3.66}$$

The derivative in the denominator can be approximated by a difference quotient. That means, after we have found the T value of the pole, we have to perform one last CDF fit to obtain a and ν for a slightly shifted T value.

Imaginary Part of the Effective Action

We can now use the results obtained in the preceding sections to evaluate Eq. (3.14). The number of poles that have to be taken into account depends on the field configuration. For an inhomogeneous field distribution with maximal field strength E_{max}, the poles have larger T values than for a field of constant strength E_{max}. Consequently their residues are suppressed more and using the same number of poles one would use for the constant field yields a reliable estimate. In the case of a constant field $E\equiv\frac{m^2}{e}$, $\langle W\rangle$ has poles at $T/m^2=\pi l$, cf. Eq. (3.13). The residues' absolute values are proportional to T. Due to the factor $\frac{e^{-m^2T}}{T^3}$ in Eq. (3.14), the contribution of the second pole to $\mathrm{Im}\Gamma$ is about 1% of that of the first pole and can be neglected if the statistical error is larger than 1%. Thus, to compute the imaginary part of the effective action for the Sauter potential of the pole-position plot Fig. 3.11 with the maximal field strength $E_{\mathrm{max}}=\frac{m^2}{e}$, we only take the first pole into account.

Before we compute the imaginary part of the complete effective action, let us first study the corresponding density $\mathrm{Im}\mathcal{L}_{\mathrm{eff}}$ in the centre of the Sauter potential, which is closely related to the pole position of the Wilson-loop expectation value shown in Fig. 3.11. Figure 3.12 shows $\mathrm{Im}\mathcal{L}_{\mathrm{eff}}$ at $x_1=0$ against the width parameter k. It goes to zero, when k reaches m, despite the fact, that the field strength at $x_1=0$ is kept constantly equal to $\frac{m^2}{e}$. This clearly demonstrates the nonlocal nature of $\mathcal{L}_{\mathrm{eff}}$, which comes from the fact, that a loop cloud, sitting in the centre of the Sauter potential,

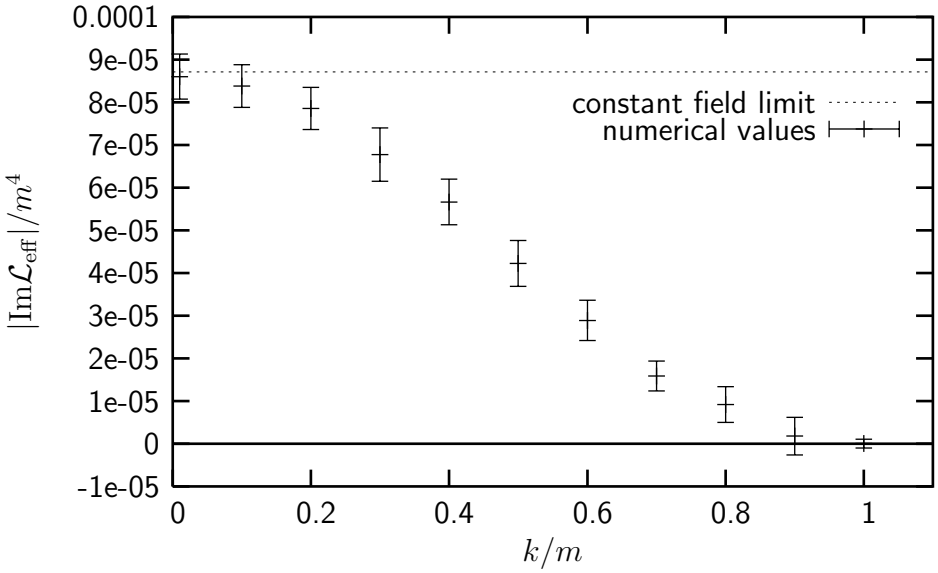

Figure 3.12: The imaginary part of the effective Lagrangian in the centre of a Sauter potential with maximal field strength $\frac{m^2}{e}$ versus the width parameter k. The dashed line marks the analytically obtained contribution of he first pole to $|\mathrm{Im}\mathcal{L}_{\mathrm{eff}}|$ for the constant field limit. $n_{\mathrm{L}} = 100000$, $N = 1000$ ppl.

gathers information not only at its centre of mass, but also from the centre's neighbourhood. There the field gets weaker, when k increases.

The density $\mathrm{Im}\mathcal{L}_{\mathrm{eff}}$ has to be integrated over all space time, in order to obtain $\mathrm{Im}\Gamma$. Only the x_1 integration has to be performed numerically, as the problem is translationally invariant in the other directions. Figure 3.13 shows the x_1 dependence of $\mathrm{Im}\mathcal{L}_{\mathrm{eff}}$ for $k = 0.4m$ and $E_{\max} \equiv ak = \frac{m^2}{e}$. It is compared to the effective Lagrangian obtained analytically, if the field is assumed to be locally constant. Again we notice a nonlocal behaviour: the locally constant field approximation is literally "washed-out" by the loop cloud. Worldline numerics yields smaller values in the centre of the potential, whereas it gives larger values at a distance from $x_1 = 0$. Finally, Fig. 3.14 shows $\frac{\mathrm{Im}\Gamma}{L^2T}$ after the numerical x_1 integration compared to the Nikishov result. With increasing width of the potential, which means an increasing quotient m/k, the imaginary part of the effective action and therewith the pair-production rate increases. The agreement with Nikishov's result is satisfactory and the vanishing pair production for $ea = m$ is reproduced. To better visualize these two points, the same quantities as in Fig. 3.14 are plot-

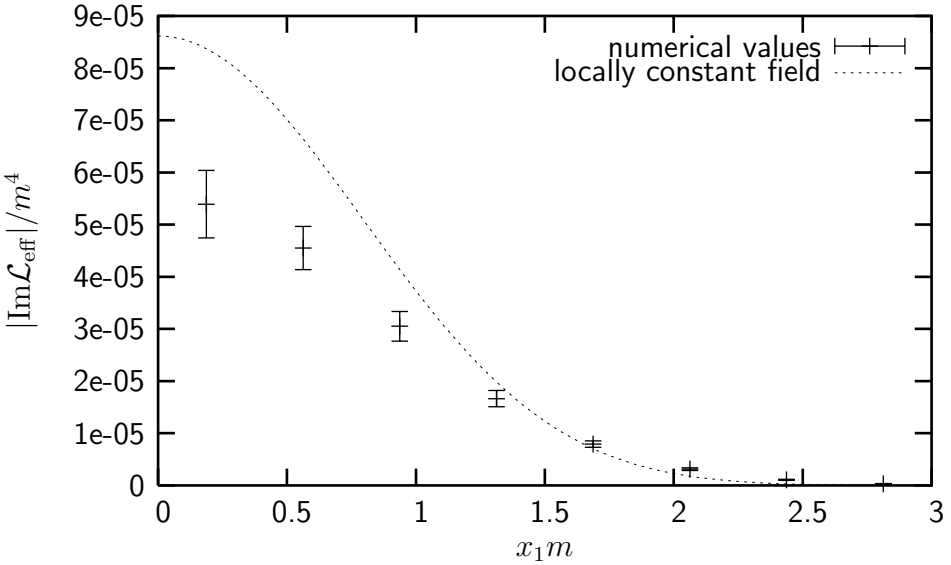

Figure 3.13: Spatial distribution of the effective Lagrangian for a Sauter potential. The numerical result is compared to the locally constant field approximation that overestimates the true result by up to $\sim 50\%$. Parameters of the Sauter potential: $k = 0.4m$, $E_{\max} = \frac{m^2}{e}$. Parameters of the loop cloud: $n_{\mathrm{L}} = 100000$, $N = 1000$ ppl.

ted as proportion of the result of the locally constant field approximation in Fig. 3.15. The numerical values reproduce the analytic result for all k while the locally constant field approximation only holds for very small k values, i.e., small spatial field variation.

3.3.5 Conclusion

With the CDF fit procedure we have developed a powerful numerical algorithm to compute the imaginary part of the effective action. The procedure is applicable for arbitrary potentials. The quality of its result depends on how good the ansatz P_{fit} in Eq. (3.55) matches the real probability distribution function for the given problem. As a generalization of the constant field result and with two free parameters controlling the main features of the PDF, our choice of P_{fit} appears to represent a very reasonable approach, which is strongly supported by the results for the Sauter potential. Thus we are prepared to turn towards field configurations for which reliable analytical treatments have not been developed so far.

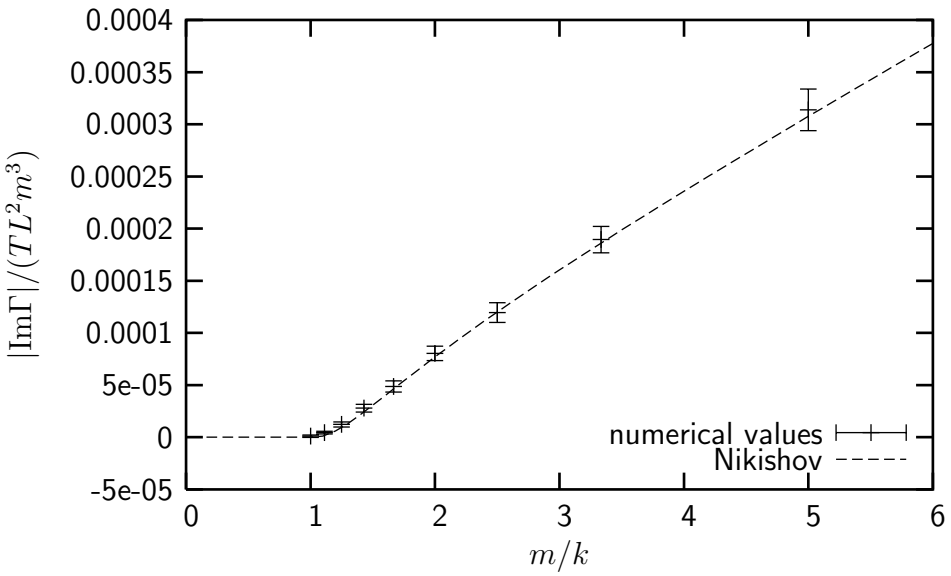

Figure 3.14: The imaginary part of the effective action of a Sauter potential versus the width $1/k$: comparison of the numerical result with Nikishov's analytic expression. $n_{\mathrm{L}} = 100000$, $N = 1000$ ppl.

3.4 Sine Potential

In this section we study the superposition of a sine potential with a constant field potential. This configuration is of general interest, as it is representative for a class of field configurations, which are a superposition of a slowly varying field–in our example the constant field–and high-frequency modes. A very important aspect is the dependence of the pair-production rate on the frequency of the small scale field-structures. We will use our simple example configuration to study this question with the intention to identify conclusions of more general validity.

In Minkowski space the potential is given by

$$A^0_{\mathrm{M}} = -a \sin kx^1 - E_0 x^1, \tag{3.67}$$

$$A^i_{\mathrm{M}} = 0, \quad i = 1, 2, 3. \tag{3.68}$$

It corresponds to an E field in x^1 direction with field strength

$$E^1_{\mathrm{M}} = E_0 + ak \cos kx^1, \tag{3.69}$$

which reaches the maximal field strength $E_{\max} = E_0 + ak$. By studying the dependence of the pair production on the frequency k of the sine, we

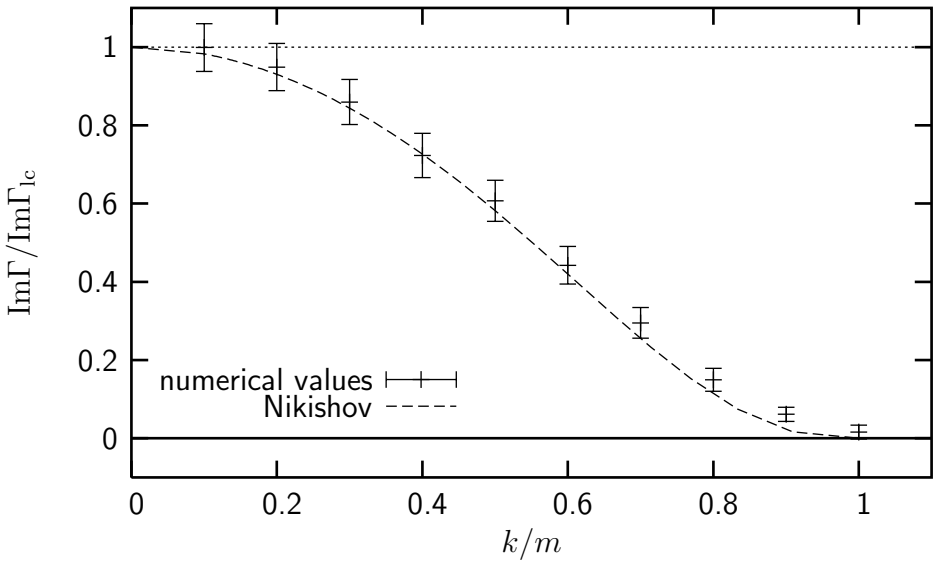

Figure 3.15: The imaginary part of the effective action of a Sauter potential as fraction of the locally constant field approximation $\mathrm{Im}\Gamma_{\mathrm{lc}}$ versus the width parameter k: comparison of the numerical result with Nikishov's analytic expression. $n_{\mathrm{L}} = 100000$, $N = 1000$ ppl.

obtain information about the qualitative and quantitative influence of spatial inhomogeneities.

Before performing the CDF algorithm, let us shortly discuss the two extreme cases $k = 0$ and $k \to \infty$. For small k and a slowly varying field, the effective action density is well approximated if the field is regarded as locally constant using the Schwinger formula. In the opposite limit, if k goes to infinity and the field fluctuates rapidly around the constant field E_0, we expect to obtain the pair production of this constant field. Heuristically, the "size" scale $\lambda_{\mathrm{C}} \approx \frac{1}{m}$ of a virtual pair cannot resolve the spatial inhomogeneities with $k \gg m$. Thus the pair production rate should be obtainable by averaging over the field strength and computing the effective action afterwards. On the other hand, for small k, the calculation corresponds to first computing the effective action density and averaging in the second place, to obtain the pair production per space-time volume. The differing pair-production rate that we expect for the two extreme cases, immediately raises the question how it devolves from one value to the other and in which range of k the transition takes place.

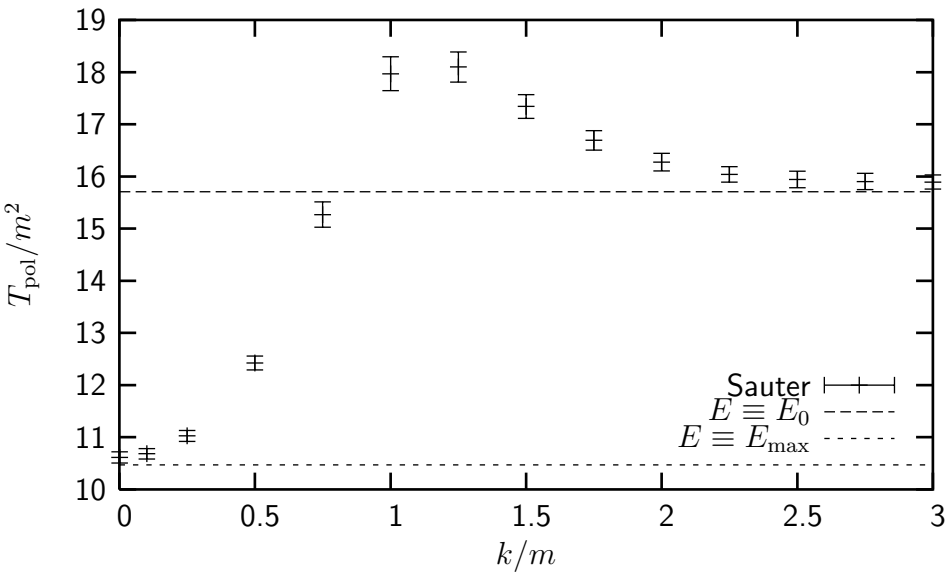

Figure 3.16: Position of the first pole of $\langle W \rangle$ at a maximum of the field strength. With increasing frequency k, the pole moves from the constant field limit $E \equiv E_{\rm max}$ to the limit $E \equiv E_0$. Parameters of the field: $E_0 = 0.2\frac{m^2}{e}$, $E_{\rm max} = 0.3\frac{m^2}{e}$. In between, it develops an unexpected maximum corresponding to a minimum of the local production rate. Parameters of the loop cloud: $n_{\rm L} = 100000$, $N = 1000$ ppl.

As an example, we study a field with $E_0 = 0.2\frac{m^2}{e}$ and $E_{\rm max} = 0.3\frac{m^2}{e}$. In this case, the pair production rate is dominated by the first pole contribution, and as in the previous section we can safely neglect the remaining poles. Figure 3.16 shows the position of the first pole of the Wilson loop expectation value in the centre of a maximum of the field strength. For small k, the constant-field limit $E \equiv E_{\rm max}$ is reproduced. For large k, the pole position converges to the result of the averaged field $E \equiv E_0$. In between, the curve is not monotonically increasing, as one might have expected, but reaches T values which are significantly larger than in both constant-field limits. As a consequence, the corresponding density of the imaginary part of the effective action will be smaller than in the constant-field limit $E \equiv E_0$. One might assume, that if the density at a *maximum* of the field strength is smaller than for the averaged field, the total pair production will also be smaller. Before resolving this question, let us study the origin of the somewhat surprising behaviour of the pole.

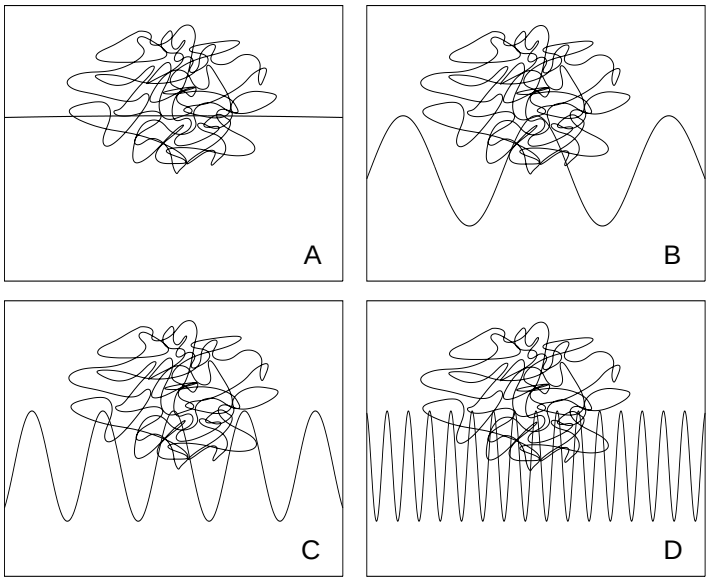

Figure 3.17: Sketch of a loop cloud at a maximum of the field strength. For small frequencies, it detects only the maximum (A). After increasing the frequency, the two nearest minima dominate (B). For larger frequencies the cloud encounters further maxima (C), until it perceives an averaged field (D).

Starting with the limit $k \to 0$, a loop cloud sitting at a maximum detects a constant field of strength $E_{\max}$. A sketch of this scenario if given in Fig. 3.17.A. If k is increased and the wavelength of the sine becomes shorter, the loop cloud more and more overlaps with the minima on each side of the maximum and the pole moves to larger T values. If k exceeds a certain value, in our example at about $k = 0.8m$, the two close-by minima dominate the Wilson loop expectation value, Fig. 3.17.B, and despite the maximum in the centre of the loop cloud, the pole is at a larger T value than for the averaged field. Not until the loop cloud approaches the adjacent maxima, Fig. 3.17.C, the T value becomes smaller again, to finally converge to the value of the averaged field, Fig. 3.17.D. Since the Wilson loop expectation value at a maximum of the field strength can be dominated by the adjacent minima, also the inverse situation can occur at a minimum, where the result can be dominated by the two adjacent maxima. In this case, the first pole of $\langle W \rangle$ is at a *smaller* T value than for the averaged field, leading to a *larger* imaginary part of the effective Lagrangian. This inversion is shown in Fig. 3.18, where the spatial distribution of the imaginary part of the

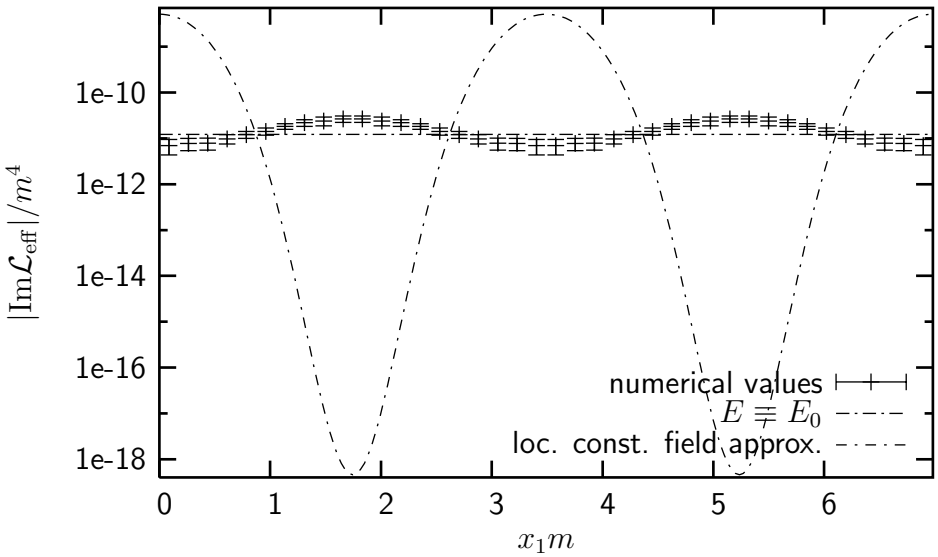

Figure 3.18: Spatial distribution of the imaginary part of the effective-action density for the sine potential with $k = 1.8m$, compared to the locally constant-field approximation and the constant field limit $E \equiv E_0$. $n_{\mathrm{L}} = 200000$, $N = 1000$ ppl.

effective action for $k = 1.8m$ is plotted, compared to the locally constant-field approximation and the constant-field limit $E \equiv E_0$.

Figure 3.19 shows the imaginary part of the total effective action per space-time volume for our example configuration versus the frequency k. In contrast to its density at x_0, ImΓ does not fall below the result for the averaged field. Starting with the result of the locally constant field approximation at $k = 0$, we obtain the constant field limit $E \equiv E_0$ for large frequencies. It is remarkable, that the imaginary part of the effective action reaches the value of the averaged field for k values as small as about $k = m$, whereas its density still fluctuates spatially for even larger k values, as we have seen in Fig. 3.18. The fluctuations cancel each other, so that they have no effect on the integrated quantity. The numerical accuracy does not eliminate the possibility of a k-dependent structure for k values larger than m. According to the values of Fig. 3.18, one actually might assume a slight increase of the pair production for $k > m$, until it falls back to the result for the averaged field if $k/m \to \infty$. To definitely clarify this, the PDF fit has to be rerun with a larger loop ensemble, at the expense of CPU time. However, the

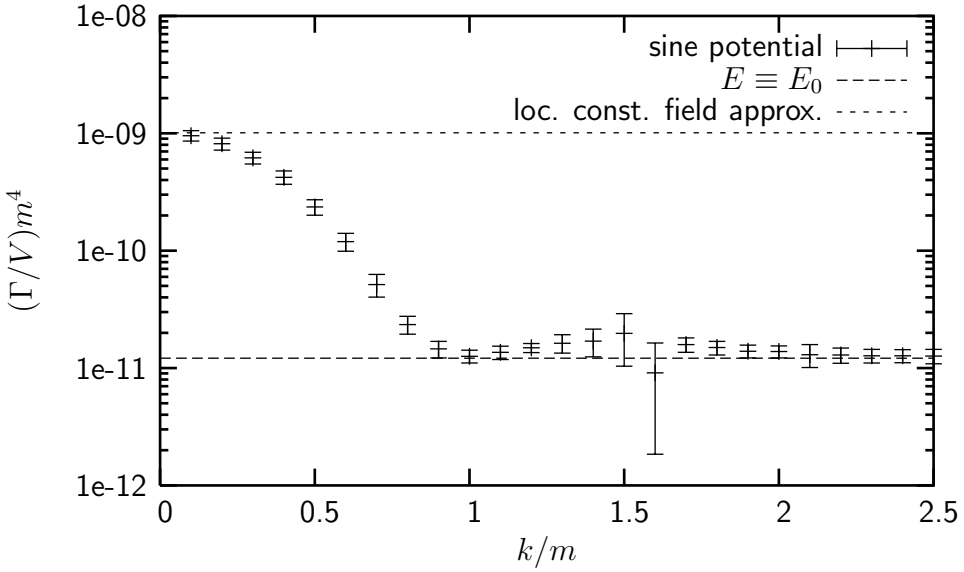

Figure 3.19: The imaginary part of the total effective action per space-time volume against the frequency k. The dashed lines mark the locally constant-field approximation and the result for the averaged field $E \equiv E_0$, respectively. $n_{\mathrm{L}} = 200000$, $N = 1000$ ppl.

present result shows, that any possible k dependence for $k > m$ has to be relatively small and the averaged-field approximation yields good results in this range. On the other hand, Figure 3.19 shows that the locally constant field approximation yields proper results only for very small frequencies, i.e., a very slowly varying field.

We obtained two remarkable results: Firstly we found, that for certain values of k the imaginary part of effective Lagrangian is largest at the minima of the field strength and smallest at the maxima. This is very notable, since the effective Lagrangian corresponds to the local pair-production rate. That means, we expect more pairs to be produced where the field is weakest than in regions of maximal field strength! Beyond the quantitative result, the underlying worldline formalism provides us with a vivid qualitative understanding of this nonlocal phenomenon in terms of loop clouds. Our second major result is the range of validity for the averaged field approximation, where the small-scale structures of the field are averaged out and the remaining field is treated as locally constant. We have expected it to be valid, if the wavelength of the sine becomes much shorter than the Compton wavelength

of the produced particles, i.e., if $k \gg m$. Instead, we found it to provide satisfying results for $k \gtrsim m$. Despite the fact that we have treated only a special field configuration, we can conclude that, for any field consisting of a slowly varying component of the same order of magnitude as our constant field $E_0 = 0.2\frac{m^2}{e}$ and spatial fluctuations with an amplitude of about $0.1\frac{m^2}{e}$, the averaged field approximation is valid, provided that the characteristic length scale of the fluctuations is smaller than the Compton wavelength of the created particles.

3.5 Steepest-Descent Approach to Pair Production

A method to approximately obtain the pair production on the worldline based on instanton techniques has been presented in [47]. The basic idea is to interchange the T integral and the path integral in expression (2.29) and compute both in the steepest-descent approximation. After rescaling T and τ, Eq. (2.29) reads

$$\Gamma^1 = -\int_0^\infty \frac{dT}{T}\mathcal{N}\int \mathcal{D}x e^{-\frac{m^2}{2}T-\frac{1}{2T}\int_0^1 d\tau\dot{x}^2-ie\oint dxA} \tag{3.70}$$

$$= -\mathcal{N}\int \mathcal{D}x e^{-ie\oint dxA}\int_0^\infty \frac{dT}{T}e^{-(\frac{m^2}{2}T+\frac{1}{2T}\int_0^1 d\tau\dot{x}^2)}. \tag{3.71}$$

The exponent in the T integral has a minimum at $T_0^2 = \int \dot{x}^2/m^2$. Assuming $m^2\int_0^1 \dot{x}^2 \gg 1$, the steepest-descent approximation yields

$$\Gamma^1 = -\frac{1}{m}\sqrt{\frac{2\pi}{T_0}}\mathcal{N}\int \mathcal{D}x\ e^{-S}, \tag{3.72}$$

where we introduced the action $S = m\sqrt{\int \dot{x}^2} + ie\oint dxA$. This action is stationary if

$$\frac{m\ddot{x}_\mu}{\sqrt{\int \dot{x}^2}} = -eF_{\mu\nu}\dot{x}_\nu. \tag{3.73}$$

For the constant E field, $F_{34} = -F_{43} = E$, the action has a minimum for the worldline instanton

$$x^{cl} = \frac{m}{eE}(0, 0, \cos 2\pi\tau, \sin 2\pi\tau) \tag{3.74}$$

with $S[x^{cl}] = \pi\frac{m^2}{eE}$. This is already the correct exponent of the first term in the Schwinger pair-production rate Eq. (3.15). The quadratic order of the expansion of S about x^{cl} gives the correct imaginary prefactor, as shown in [47], and the steepest-descent approximation yields

$$\mathrm{Im}\Gamma = \frac{(eE)^2}{16\pi^2} e^{-\pi\frac{m^2}{eE}}, \tag{3.75}$$

which is exactly the first-pole contribution to the Schwinger pair-production rate. Further terms of the series are obtained with multi-instantons with higher winding numbers.

It is very remarkable that one single circular path gives the correct exponential dependence of the first term of the Schwinger pair-production rate, whereas the small fluctuations around this path lead to the correct imaginary prefactor. In comparison to this, the loops we use for our numerical computations seem to be extraordinary complex. Not a single loop in our ensembles has resemblance with a circle or fluctuations thereof. This gives rise to the conjecture that the computation of the imaginary part requires very little information about the shape of the loops. We expect that we should be able to extract the instantonic content of our loops by a suitable cooling procedure. Since cooling removes "UV noise", i.e., high-frequency fluctuations of the loops, only low-frequency information seems to be relevant for pair-production. This agrees with our observation that pair production is induced by "large" loops that can acquire enough energy in the E field. Therefore, it is well possible that a different loop discretization which optimizes IR properties allows for an even more efficient computation of the imaginary part. A further investigation of this topic might lead to a more profound understanding of worldline numerics.

Chapter 4

Conclusions and Outlook

Pair production in quantum field theory is a vital subject both in experimental and in theoretical physics. However, the application of established theoretical methods is restricted to special cases. In this thesis we have developed a new universal approach. It is based on the combination of the worldline formalism with Monte Carlo techniques.

We have used the constant pure electric field in scalar QED as a laboratory for the development of an algorithm to compute pair-production rates in more general backgrounds. However, during the treatment of this simple example, we have come across a result of general importance. As we have noticed in section 3.2.3, the use of pure worldline numerics for weak electric fields is limited by the size of the employed loop ensemble. Only unit loops that exceed a certain minimal extension contribute to the pair production: the integral $I = \int_0^1 dt \dot{y}_4 y_1$ has to fulfill the condition $|I| > E_{\mathrm{cr}}/E$. In a *finite* loop ensemble the $|I|$ values are bounded, so that for a sufficiently small field strength E no loop at all contributes to the pair-production rate. To still access weak field configurations, only very few reasonable assumptions of physical nature have been necessary to deduce relevant information from the finite loop ensemble.

Our efforts have resulted in a universal algorithm, the *CDF-fit* procedure, which has been introduced in section 3.3.3. With use of this algorithm, we have not only recovered Nikishov's analytic result for the total pair-production rate in a Sauter potential, but moreover we have computed the distribution of the local pair-production rate for this classic case. The CDF-fit algorithm is not restricted to any symmetry of the given background potential. In fact, it is applicable for arbitrary potentials.

As an example we have applied the developed CDF-fit algorithm to the potential of a constant electric field superimposed by a sine potential. This field configuration is representative for a whole class of fields with large-scale structures and small scale fluctuations. Concerning the local pair-production rate, for an appropriate frequency of the sine we found the remarkable situation, in which the rate is largest in the minima of the field strength whereas it is smallest where the field is strongest. We have also studied the total pair production rate as a function of the sine's frequency. For small frequencies, our numerical result agrees with the derivative expansion to lowest order. More remarkable is the behaviour for high frequencies: already for relatively large wave lengths of the same order of magnitude as the Compton wave length of an electron, the result of the CDF-fit algorithm agrees with the pair-production rate corresponding to the averaged field. This finding suggests, that for many field configurations the correct pair-production rate is obtained by averaging out small-scale fluctuations of the background field to perform a derivative expansion on the averaged field.

So far, we have concentrated on pair production in *scalar* QED. For the algorithms we developed for the constant field, a generalization to spinor QED is a straightforward task. The extra term (2.78) has to be taken into account when computing the Wilson loop. However, in the CDF-fit algorithm the Wilson loop values are never computed explicitly. A straightforward (though CPU consuming) generalization is nevertheless possible by determining the CDFs depending now on two variables: the quantity I, as before, and the additional spin-field coupling term. The total result then follows by integrating over the distributions of both quantities.

As already noted, the CDF-fit algorithm is applicable for arbitrary potentials. This also includes time dependent potentials. But, as we have performed all calculations in Euclidean space, the potential must be known on the imaginary time axis. Provided that the time dependence of the potential is given analytically, the CDF-fit should be of use when studying time dependent fields.

Our approach yields the instantaneous pair-production rate, back-reactions and memory effects are neglected. However, as we have mentioned in the introduction, the results of our algorithm can be used as input for transport equations, which take these effects into account.

From a technical perspective, we have been able to solve a strong "overlap" problem by extrapolating the probability distribution of I to large val-

ues. Similar approaches can be useful to tackle overlap problems that occur in a different context. Also the ability of our algorithm to compute the imaginary part of functional determinants should be of general numeric interest, for instance, for fermionic determinants in thermal field theory with nonzero chemical potential.

Appendix A

Numerical Tools

A.1 The VLoop Algorithm

Let us review the vloop algorithm that was originally introduced in [30]. It is based on a linear variable transformation $\{y_k\} \to \{\bar{v}_k\}$, such that the discretized distribution (2.61) becomes purely Gaußian. These new variables are velocity-like and diagonalize the quadratic form in the exponent.

Because of the δ function in Eq. (2.61), only $N-1$ coordinates per loop are independent. Defining $\int \mathcal{D}y = \int_{-\infty}^{\infty} \prod_{i=1}^{N} dy_i$, we may perform, e.g., the y_N integration using the δ function,

$$\begin{aligned} & \int \mathcal{D}y\, P\big[\{y_k\}\big] \dots \\ = & \int \prod_{i=1}^{N-1} dy_i \; e^{\left[-\frac{N}{4}\left(\sum_{i=2}^{N-1}(y_i-y_{i-1})^2+(2y_1+y_2+\cdots+y_{N-1})^2+(y_1+y_2+\cdots+2y_{N-1})^2\right)\right]} \dots \\ =: & \int \prod_{i=1}^{N-1} dy_i \; e^{\left[-\frac{N}{4}Y\right]} \dots, \end{aligned} \tag{A.1}$$

where the dots represent an arbitrary y-dependent operator, and we introduced the abbreviation Y for the quadratic form. In order to turn the exponential into a product of simple Gaußians, we define $N-1$ new velocity-like variables,

$$\begin{aligned} \bar{v}_1 &:= \frac{3}{2}y_1 + y_2 + y_3 + \cdots + y_{N-2} + \frac{3}{2}y_{N-1}, \\ v_i &:= y_i - y_{i-1}, \quad i = 2, 3, \dots, N-1. \end{aligned} \tag{A.2}$$

For notational simplicity, it is useful to also introduce the auxiliary variable,

$$v_{i,j} = v_i + v_{i-1} + \cdots + v_{j+1} \equiv y_i - y_j, \quad \text{for } i \geq j = 1, 2, \ldots, N-1, \quad \text{(A.3)}$$

such that the exponent Y can be written as

$$\begin{aligned} Y &= \sum_{i=2}^{N-1} v_i^2 + \left(\bar{v}_1 - \frac{1}{2} v_{N-1,1}\right)^2 + \left(\bar{v}_1 + \frac{1}{2} v_{N-1,1}\right)^2 \\ &= 2\bar{v}_1^2 + \frac{1}{2} v_{N-1,1}^2 + \sum_{i=2}^{N-1} v_i^2. \end{aligned} \quad \text{(A.4)}$$

We observe that the variable $\bar{v}_1$ now appears quadratically in the exponent as desired. The same has still to be achieved for $v_2 \ldots v_{N-1}$. For this, we note that $v_{N-1,1} = v_{N-1} + v_{N-2,1}$ by definition (A.3). Defining

$$\bar{v}_{N-1} := v_{N-1} + \frac{1}{3} v_{N-2,1}, \quad \text{(A.5)}$$

we indeed obtain for the exponent Y

$$\begin{aligned} Y &= 2\bar{v}_1^2 + v_{N-1}^2 + \frac{1}{2}(v_{N-1} + v_{N-2,1})^2 + \sum_{i=2}^{N-2} v_i^2 \\ &= 2\bar{v}_1^2 + \frac{3}{2}\bar{v}_{N-1}^2 + \frac{1}{3} v_{N-2,1} + \sum_{i=2}^{N-2} v_i^2, \end{aligned} \quad \text{(A.6)}$$

where $\bar{v}_{N-1}^2$ also appears quadratically. We can continue this construction by defining

$$\bar{v}_{N-i} := v_{N-i} + \frac{1}{i+2}\, v_{N-i-1,1}, \quad i = 1, \ldots, N-2\,, \quad \text{(A.7)}$$

which turns the exponent Y into a purely Gaußian form:

$$Y = 2\bar{v}_1^2 + \frac{3}{2}\bar{v}_{N-1}^2 + \frac{4}{3}\bar{v}_{N-2}^2 + \cdots + \frac{i+2}{i+1}\bar{v}_{N-i}^2 + \cdots + \frac{N}{N-1}\bar{v}_2^2. \quad \text{(A.8)}$$

The last step of this construction consists in noting that we can substitute the integration variables according to

$$\prod_{i=1}^{N-1} dy_i = J \prod_{i=2}^{N-1} dv_i d\bar{v}_1 = \bar{J} \prod_{i=1}^{N-1} d\bar{v}_i \equiv \mathcal{D}\bar{v} \quad \text{(A.9)}$$

with nonzero but constant Jacobians J, $\bar{J}$, the value of which is unimportant for the calculation of expectation values. This allows us to write the path integral Eq. (A.1) as

$$\begin{aligned}\int \mathcal{D}y\, P\big[\{y_k\}\big]\ldots &= \bar{J}\int \mathcal{D}\bar{v}\ \exp\left[-\frac{N}{4}\left(2\bar{v}_1^2+\sum_{i=1}^{N-2}\frac{i+2}{i+1}\bar{v}_{N-i}^2\right)\right]\ldots \\ &\equiv \bar{J}\int \mathcal{D}\bar{v}\, P\big[\{\bar{v}_k\}\big]\ldots, \end{aligned} \tag{A.10}$$

where $P\big[\{\bar{v}_k\}\big]$ can now be generated straightforwardly with the Box-Müller method [48].

For the construction of unit loops ("v loops"), the above steps have to be performed backwards. The recipe is the following:

(1) generate $N-1$ numbers w_i, $i=1,\ldots,N-1$ via the Box-Müller method such that they are distributed according to $\exp(-w_i^2)$;

(2) compute the $\bar{v}_i$, $i=1,\ldots,N-1$, by normalizing the w_i:

$$\begin{aligned}\bar{v}_1 &= \sqrt{\frac{2}{N}}\, w_1, \\ \bar{v}_i &= \frac{2}{\sqrt{N}}\sqrt{\frac{N+1-i}{N+2-i}}\, w_i, \quad i=2,\ldots,N-1\,; \end{aligned} \tag{A.11}$$

(3) compute the v_i, $i=2,\ldots,N-1$, using

$$v_i = \bar{v}_i - \frac{1}{N+2-i}\, v_{i-1,1}, \quad \text{where } v_{i-1,1}=\sum_{j=2}^{i-1} v_j\,; \tag{A.12}$$

(4) construct the unit loops according to

$$\begin{aligned} y_1 &= \frac{1}{N}\left(\bar{v}_1-\sum_{i=2}^{N-1}\left(N-i+\frac{1}{2}\right)v_i\right), \\ y_i &= y_{i-1}+v_i, \quad i=2,\ldots,N-1, \\ y_N &= -\sum_{i=1}^{N-1} y_i\,; \end{aligned} \tag{A.13}$$

(5) repeat this procedure n_{L} times for n_{L} unit loops.

The formulas in step (4) can be checked straightforwardly by inserting the definitions of the v_i's and $\bar{v}_1$.

This v-loop algorithm allows us to generate unit loops very efficiently and works for an arbitrary number of points per loop N. For further techniques to generate loop ensembles with the desired distribution see [30].

A.2 Jackknife Error Estimation

Let us briefly review the jackknife method. Consider a not very large sample of N_s independent measurements of a primary quantity A. The measured values are $A_1, A_2, \cdots, A_{N_\mathrm{s}}$. The best estimate of an arbitrary secondary quantity y is $y(\bar{A})$, where $\bar{A}$ denotes the arithmetic average of the sample. To obtain an error estimate for $y(\bar{A})$ we compute the *jackknife averages* $\bar{A}_{\mathrm{J}i}$, which are defined as the averages of the samples obtained by omitting a single measurement A_i from the original sample. We get N_s *jackknife estimates* $y(\bar{A}_{\mathrm{J}i})$ with the average $\bar{y_J}$. The variance of y is then estimated by $N_\mathrm{s} - 1$ times the variance of the jackknife estimates,

$$\sigma^2 = \frac{N_\mathrm{s} - 1}{N_\mathrm{s}} \sum_{i=0}^{N_\mathrm{s}} (y(\bar{A}_{\mathrm{J}i}) - \bar{y_J})^2. \tag{A.14}$$

In our context we apply this method as follows. The loop ensemble is split into N_s subensembles. The CDF of the complete loop ensemble then is the average of the subensembles' CDFs which correspond to the measurements $A_1, A_2, \cdots, A_{N_\mathrm{s}}$. The jackknife estimates of a secondary quantity like the pole position are computed by omitting one subensemble from the complete ensemble and rerunning the procedure used to obtain the secondary quantity. In case of the pole search, this would imply running the search routine N_s times. But for a reliable error estimate one should use $N_\mathrm{s} \geq 50$. If the pole position has the same order of magnitude as in the case of the constant E field, its error is about the same as the error of the estimated position in the last iteration of the search. To obtain this quantity, we only have to run one fitting procedure for each jackknife estimate. However, if a pole is found at a T value significantly larger than in the case of a constant E, this simplification gives too small error estimates.

Bibliography

[1] F. Sauter. Über das Verhalten eines Elektrons im homogenen elektrischen Feld nach der relativistischen Theorie Dirac's. *Z. Phys.*, 69:742–764, 1931.

[2] W. Heisenberg and H. Euler. Consequences of dirac's theory of positrons. *Z. Phys.*, 98:714–732, 1936.

[3] V. Weisskopf. *Kong. Dans. Vid. Selsk. Math-fys. Medd.*, XIV:166, 1936.

[4] Julian S. Schwinger. On gauge invariance and vacuum polarization. *Phys. Rev.*, 82:664–679, 1951.

[5] S. W. Hawking. Black hole explosions. *Nature*, 248:30–31, 1974.

[6] Thibault Damour and Remo Ruffini. Quantum electrodynamical effects in kerr-newman geometries. *Phys. Rev. Lett.*, 35:463, 1975.

[7] Sang Pyo Kim and Don N. Page. Remarks on schwinger pair production by charged black holes. 2004.

[8] A. Casher, H. Neuberger, and S. Nussinov. Chromoelectric flux tube model of particle production. *Phys. Rev.*, D20:179–188, 1979.

[9] Leonard Parker. Quantized fields and particle creation in expanding universes. 1. *Phys. Rev.*, 183:1057–1068, 1969.

[10] B. Garbrecht and T. Prokopec. Energy density in expanding universes as seen by unruh's detector. *Phys. Rev.*, D70:083529, 2004.

[11] E. Brezin and C. Itzykson. Pair production in vacuum by an alternating field. *Phys. Rev.*, D2:1191–1199, 1970.

[12] W. Greiner and J. Reinhardt. Quantum aspects of beam physics. proceedings, advanced icfa beam dynamics workshop, monterey, usa, january 4-9, 1998. page 438. Prepared for 15th Advanced ICFA Beam Dynamics Workshop on Quantum Aspects of Beam Physics, Monterey, California, 4-9 Jan 1998.

[13] J. Arthur et al. Linac coherent light source (lcls) design study report. SLAC-R-0521.

[14] (ed.) Materlik, G. and (ed.) Tschentscher, T. Tesla: The superconducting electron positron linear collider with an integrated x-ray laser laboratory. technical design report. pt. 5: The x-ray free electron laser. DESY-01-011.

[15] (ed.) Brinkmann, R. et al. Tesla xfel: First stage of the x-ray laser laboratory. technical design report, supplement. DESY-02-167.

[16] A. Ringwald. Boiling the vacuum with an x-ray free electron laser. 2003.

[17] D. B. Blaschke, A. V. Prozorkevich, S. A. Smolyansky, and A. V. Tarakanov. Pulsations of the electron-positron plasma in the field of optical lasers. 2004.

[18] B. S. Dewitt. Quantum field theory in curved space-time. *Phys. Rept.*, 19:295–357, 1975.

[19] Joakim Hallin and Per Liljenberg. Fermionic and bosonic pair creation in an external electric field at finite temperature using the functional schrodinger representation. *Phys. Rev.*, D52:1150–1164, 1995.

[20] H. M. Fried and R. P. Woodard. The one loop effective action of qed for a general class of electric fields. *Phys. Lett.*, B524:233–239, 2002.

[21] J. Avan, H. M. Fried, and Y. Gabellini. Non trivial generalizations of the schwinger pair production result. *Phys. Rev.*, D67:016003, 2003.

[22] S. A. Smolyansky et al. Dynamical derivation of a quantum kinetic equation for particle production in the schwinger mechanism. 1997.

[23] S. A. Smolyansky et al. Relativistic quantum kinetic equation of the vlasov type for systems with internal degrees of freedom. *Int. J. Mod. Phys.*, E7:515–526, 1998.

[24] Yuval Kluger, Emil Mottola, and Judah M. Eisenberg. The quantum vlasov equation and its markov limit. *Phys. Rev.*, D58:125015, 1998.

[25] Sang Pyo Kim and Don N. Page. Schwinger pair production via instantons in a strong electric field. *Phys. Rev.*, D65:105002, 2002.

[26] Sang Pyo Kim and Don N. Page. Schwinger pair production in electric and magnetic fields. 2003.

[27] Holger Gies and Kurt Langfeld. Quantum diffusion of magnetic fields in a numerical worldline approach. *Nucl. Phys.*, B613:353–365, 2001.

[28] Holger Gies and Kurt Langfeld. Loops and loop clouds: A numerical approach to the worldline formalism in qed. *Int. J. Mod. Phys.*, A17:966–978, 2002.

[29] Kurt Langfeld, Laurent Moyaerts, and Holger Gies. Fermion-induced quantum action of vortex systems. *Nucl. Phys.*, B646:158–180, 2002.

[30] Holger Gies, Kurt Langfeld, and Laurent Moyaerts. Casimir effect on the worldline. *JHEP*, 06:018, 2003.

[31] L. Moyaerts, K. Langfeld, and H. Gies. Worldline approach to the casimir effect. 2003.

[32] R. P. Feynman. Mathematical formulation of the quantum theory of electromagnetic interaction. *Phys. Rev.*, 80:440–457, 1950.

[33] Alexander M. Polyakov. Gauge fields and strings. CHUR, SWITZERLAND: HARWOOD (1987) 301 P. (CONTEMPORARY CONCEPTS IN PHYSICS, 3).

[34] Matthew J. Strassler. Field theory without feynman diagrams: One loop effective actions. *Nucl. Phys.*, B385:145–184, 1992.

[35] Michael G. Schmidt and Christian Schubert. On the calculation of effective actions by string methods. *Phys. Lett.*, B318:438–446, 1993.

[36] Christian Schubert. Perturbative quantum field theory in the string-inspired formalism. *Phys. Rept.*, 355:73–234, 2001.

[37] Michael G. Schmidt and Ion-Olimpiu Stamatescu. Determinant calculations with random walk worldline loops. 2002.

[38] Michael G. Schmidt and Ion-Olimpiu Stamatescu. Determinant calculations using random walk worldline loops. *Nucl. Phys. Proc. Suppl.*, 119:1030–1032, 2003.

[39] A. I. Nikishov. Barrier scattering in field theory removal of klein paradox. *Nucl. Phys.*, B21:346–358, 1970.

[40] S. W. Hawking. Zeta function regularization of path integrals in curved space-time. *Commun. Math. Phys.*, 55:133, 1977.

[41] W. Dittrich and M. Reuter. Effective lagrangians in quantum electrodynamics. *Lect. Notes Phys.*, 220:1–244, 1985.

[42] W. Dittrich and H. Gies. Probing the quantum vacuum. perturbative effective action approach in quantum electrodynamics and its application. *Springer Tracts Mod. Phys.*, 166:1–241, 2000.

[43] Y. Kluger, J. M. Eisenberg, B. Svetitsky, F. Cooper, and E. Mottola. Fermion pair production in a strong electric field. *Phys. Rev.*, D45:4659–4671, 1992.

[44] V. I. Ritus. The lagrange function of an intensive electromagnetic field and quantum electrodynamics at small distances. *Sov. Phys. JETP*, 42:774, 1975.

[45] Gerald V. Dunne and Christian Schubert. Two-loop euler-heisenberg qed pair-production rate. *Nucl. Phys.*, B564:591–604, 2000.

[46] William H. Press, Brian P. Flannery, Saul A. Teukolsky, and William T. Vetterling. *Numerical Recipes: The Art of Scientific Computing*. Cambridge University Press, Cambridge (UK) and New York, 2nd edition, 1992.

[47] Ian K. Affleck, Orlando Alvarez, and Nicholas S. Manton. Pair production at strong coupling in weak external fields. *Nucl. Phys.*, B197:509, 1982.

[48] G.E.P. Box and M.E. Müller. A note on the generation of random normal deviates. *Annals Math. Statist.*, 29:610–611, 1958.

Danke!

Für die kompetente, motivierende und freundliche Betreuung sowie für das interessante und vielseitige Thema möchte ich mich ganz herzlich bei Holger Gies bedanken. Als weiterem Betreuer danke ich Prof. Michael G. Schmidt, der sich auch bereit erklärt hat, die Erstkorrektur zu übernehmen, ebenso wie dem Zweitkorrektor, welcher zu diesem Zeitpunkt noch nicht fest steht. Nicht zuletzt gebührt mein Dank dem Kollegen Hämmerling für die angenehme Zusammenarbeit.

In vornehmlich nichtfachlichen Belangen danke ich insbesondere Fred, Björn, Thomas, Tobi, Susi und Lotte sowie natürlich meinen Eltern und Geschwistern.

Erklärung:

Ich versichere, dass ich diese Arbeit selbstständig verfasst und keine anderen als die angegebenen Quellen und Hilfsmittel benutzt habe.

Heidelberg, den ....

Unterschrift